minerals

MDPI

Article

Pb-Pb and U-Pb Dating of Cassiterite by In Situ LA-ICPMS: Examples Spanning ~1.85 Ga to ~100 Ma in Russia and Implications for Dating Proterozoic to Phanerozoic Tin Deposits

Leonid A. Neymark [1,*], Anatoly M. Larin [2] and Richard J. Moscati [1]

[1] Denver Federal Center, United States Geological Survey, Box 25046, MS 963, Denver, CO 80225, USA; rmoscati@usgs.gov
[2] Institute of Precambrian Geology and Geochronology of Russian Academy of Sciences, 2 Makarova emb., 199034 Saint Petersburg, Russia; larin7250@mail.ru
* Correspondence: lneymark@usgs.gov

Abstract: This paper investigates applicability of cassiterite to dating ore deposits in a wide age range. We report in situ LA-ICPMS U-Pb and Pb-Pb dating results (n = 15) of cassiterite from six ore deposits in Russia ranging in age from ~1.85 Ga to 93 Ma. The two oldest deposits dated at ~1.83–1.86 Ga are rare metal Vishnyakovskoe located in the East Sayan pegmatite belt and tin deposits within the Tuyukan ore region in the Baikal folded region. Rare metal skarn deposits of Pitkäranta ore field in the Ladoga region, Fennoscandian Shield are dated at ~1.54 Ga. Cassiterite from the Mokhovoe porphyry tin deposit located in western Transbaikalia is 810 ± 20 Ma. The youngest cassiterite was dated from the deposits Valkumei (Russian North East, 108 ± 2 Ma) and Merek (Russian Far East, 93 ± 2 Ma). Three methods of age calculations, including $^{208}Pb/^{206}Pb$-$^{207}Pb/^{206}Pb$ inverse isochron age, Tera-Wasserburg Concordia lower intercept age, and ^{207}Pb-corrected $^{206}Pb^*/^{238}U$ age were used and the comparison of the results is discussed. In all cases, the dated cassiterite from the ore deposits agreed, within error, with the established period of magmatism of the associated granitic rock.

Keywords: LA-ICPMS; cassiterite; ore deposits: U-Pb dating

check for updates

Citation: Neymark, L.A.; Larin, A.M.; Moscati, R.J. Pb-Pb and U-Pb Dating of Cassiterite by In Situ LA-ICPMS: Examples Spanning ~1.85 Ga to ~100 Ma in Russia and Implications for Dating Proterozoic to Phanerozoic Tin Deposits. *Minerals* **2021**, *11*, 1166. https://doi.org/10.3390/min11111166

Academic Editor: Yamirka Rojas-Agramonte

Received: 24 August 2021
Accepted: 14 October 2021
Published: 22 October 2021

1. Introduction

Cassiterite (SnO_2), a main ore mineral in tin deposits, is suitable for in situ U-Pb isotopic dating using laser ablation inductively coupled plasma mass spectrometry (LA-ICPMS) because of its relatively high U/Pb ratios and typically low initial "common" Pb (Pb_c). This has been demonstrated in a series of publications within the last decade (e.g., [1–16]. Also, Neymark et al. [13] showed that Proterozoic low-Th cassiterites can be dated by an inverse Pb-Pb isochron approach using 208Pb as a common Pb proxy. Cassiterite is highly resistant to acid dissolution [17], which makes it difficult to achieve the complete acid digestion and spike homogenization needed for accurate isotope dilution and thermal ionization mass spectrometry (ID-TIMS) U-Pb dating. However, several recent publications [18–20] showed that complete dissolution of cassiterite and reliable ID-TIMS dating results are achievable. These publications provide the basis for the usage of better characterized matrix-matched reference materials for in situ analyses of cassiterite.

Tin reserves in Russia were estimated at 350,000 metric tons or 7.5 percent of world tin reserves in 2016 [21]. Tin in Russia is mined at both primary (lode) and secondary (placer) deposits. Unlike the situation in most other major producing countries (e.g., Malaysia, Indonesia, Nigeria, Brazil), in Russia the overwhelming majority of reserves is found not in placers, but in primary ores in lode deposits [22]. Approximately 95% of Russia's known tin reserves are located in its Far East economic region [23,24]. Additional tin-bearing deposits of less economic significance are known to exist in the Russian Karelia (the historic mining district of Pitkäranta) and in Siberia (e.g., the East Sayan and Baikal region).

Constraining the age of tin mineralization is critical for developing robust genetic models of the deposits. Previously published geochronology of tin/rare metal deposits in Russia used dating of spatially related granites and/or minerals coexisting with tin ore (e.g., [25–36]).

In this paper, we report the first LA-ICPMS Pb-Pb and U-Pb ages for cassiterite from several tin and rare metal deposits in Russian Karelia, Siberia, and the Russian far east obtained using previously dated by ID-TIMS primary matrix-matched reference materials. Replicate analyses of a secondary matrix-matched material were used to estimate external age uncertainty of the reported age values. The results are used to provide recommendations for the LA-ICPMS U-Pb dating of the Proterozoic and Phanerozoic cassiterite.

2. Geological Setting, Previous Geochronology, and Samples

We analyzed cassiterite from tin-bearing deposits located in six ore regions in Russian Karelia, Siberia, and the Russian far east (Figure 1). Data for two of these regions have been published previously (Tuyukan ore region and Valkumei tin deposit [13,16]) and are included here for comparison with the new dating results.

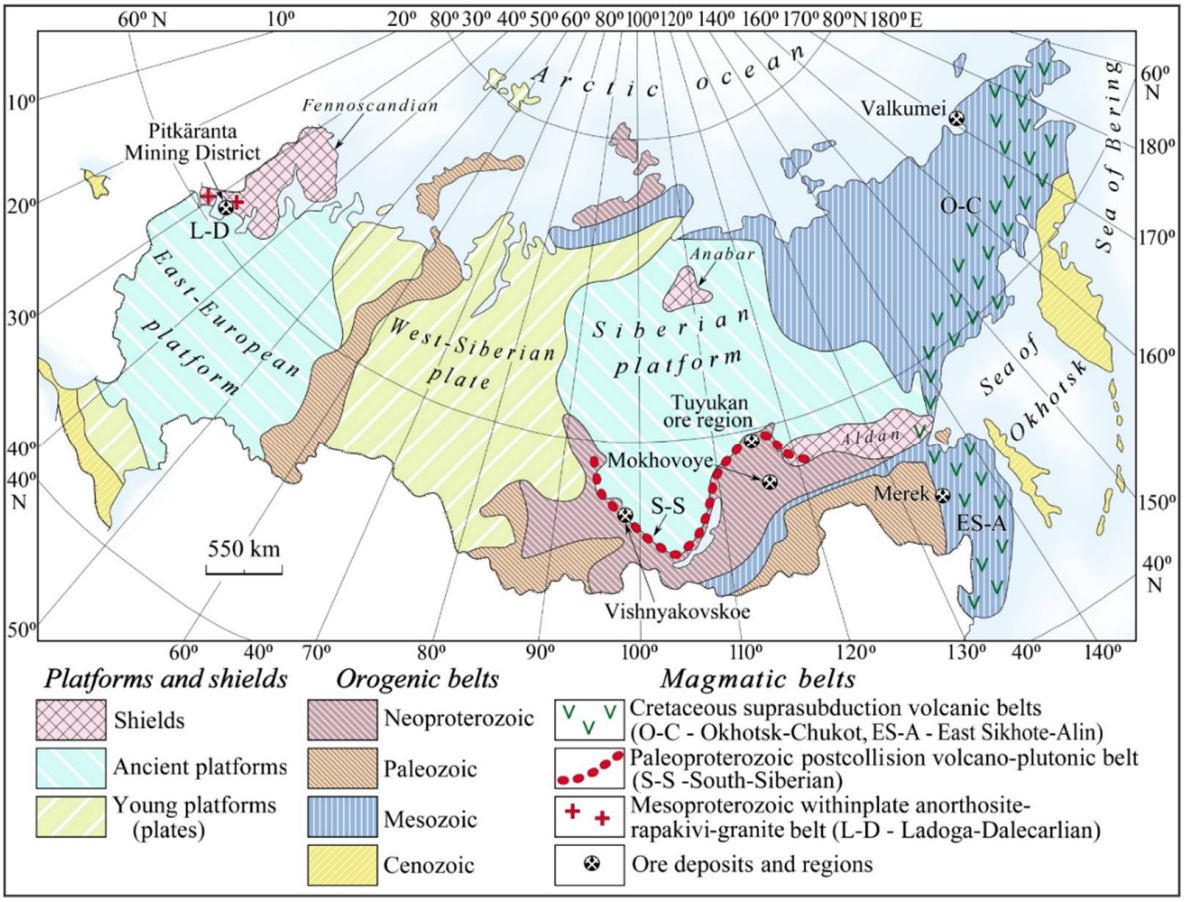

Figure 1. Simplified tectonic map of Russia showing locations of studied ore deposits. Modified from [37].

The tin ore deposits discussed in this paper differ in age, composition, and the nature of the associated granitoids of variable geochemical types formed in different geodynamic settings. The Pitkäranta mining district deposits are associated with the rocks of the anorthosite-rapakivi-granite magmatic association formed in an intraplate geodynamic setting. The Salmi batholith, which contains highly differentiated Li-F granites, is a part of the Ladoga-Dalekarlian magma belt (1.66–1.53 Ga), which stretches along the southern boundary of the Fennoscandian shield for almost 2000 km [38]. Deposits of rare metal pegmatites of the East Sayan belt [39] and tin ore deposits of the Tuyukan ore region are

associated with granite batholiths of the transregional South Siberian post-collision belt (1.88–1.84 Ga), stretching over the southern margin of the Siberian craton for more than 2500 km [40,41]. The belt is dominated by S- and A-type granites, sometimes forming bimodal magmatic associations with mafic rocks. The Mokhovoe deposit is associated with a granite-rhyolite volcano-plutonic association with geochemical characteristics of S-type granites formed during the final accretionary stage of the Baikal-Muya orogen of the Central Asian fold belt [42,43]. The deposits of the Russian Far East and North-East, Merek and Valkumei, are associated with the activity of the late Mesozoic Pacific active continental margin of the North Asian continent [44,45].

2.1. Vishnyakovskoe Rare Metal Ore Deposit

The Vishnyakovskoe large rare-metal (Ta, Li, Be, Sn, Rb, Cs) ore deposit is located in the northwestern part of the East Sayan pegmatite belt, which stretches for more than 500 km along the southwestern boundary of the Siberian Craton (Figure 2) and includes several pegmatite fields. The Vishnyakovskoe pegmatite field lies in northwest part of the belt and is located within the Paleoproterozoic Elashsky graben near the contact with the granite of the Sayan complex [46]. The deposit contains the highest quality of tantalum ores in Russia [47]. Pegmatite veins are found in ortho-amphibolites and are characterized by gentle bedding. They form vein series, where individual bodies are up to two km long and up to 12 m thick. The main ore minerals of pegmatites are represented by manganotantalite, ixiolite, wodginite, columbite, microlite, spodumene, petalite, montebrasite, eucryptite, lepidolite, cassiterite, rynersonite, and beryl [48].

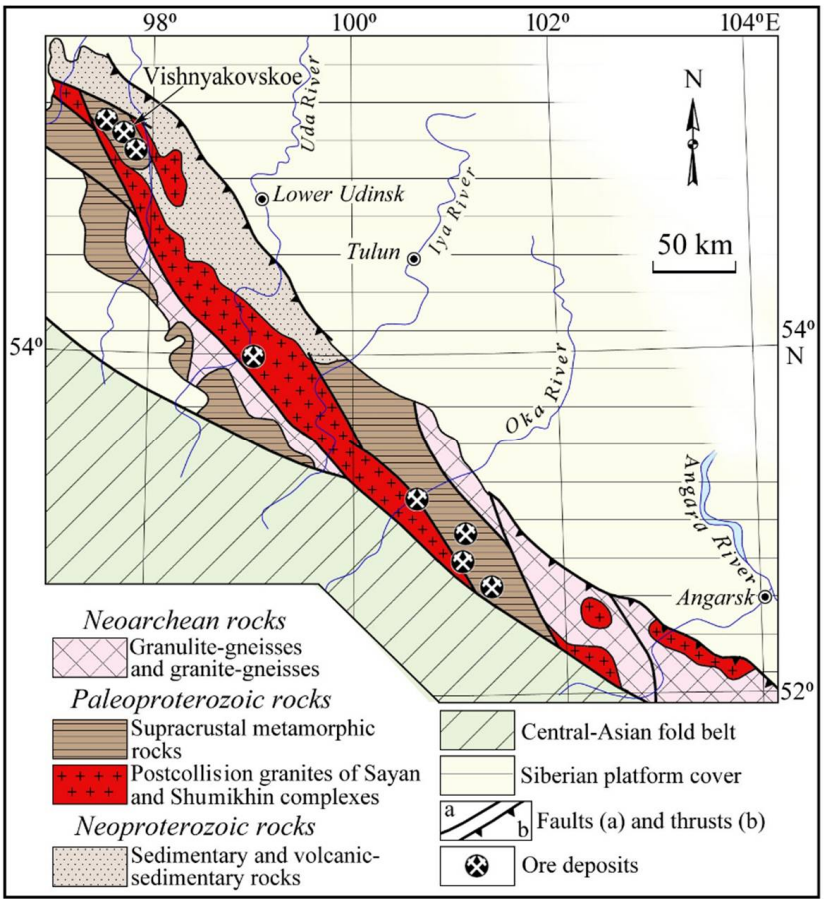

Figure 2. The East Sayan belt of rare metal pegmatites, eastern Siberia (modified from Sal'nikova et al. [48]).

The Sayan complex is composed of granitoids of two intrusive phases. The first phase is represented by biotite—amphibole granodiorites and granites; the second one, biotite and two-mica granites, biotite, muscovite, and tourmaline-containing leucogranites, pegmatitic, and aplitic veins. The geochemical characteristics of these granites correspond to the post-collisional S-type granites. The U-Pb zircon ages of the Sayan complex granites range from 1869 ± 6 to 1855 ± 5 Ma [49]. Makagon et al. [50] published Rb-Sr ages of 1490 Ma and 1480 Ma for pegmatites of the Vishnyakovskoe deposit and associated metasomatic rocks, respectively. More recently, Sal'nikova et al. [48] reported an older ID-TIMS U-Pb age of 1838 ± 3 Ma for manganotantalite from rare metal pegmatites at the Vishnyakovskoe deposit. The studied cassiterite sample 2622 was also separated from rare metal pegmatites at the Vishnyakovskoe deposit.

2.2. Tonod Uplift Quartz-Vein Tin Deposits

Tin ore deposits of the Tuyukan ore region are associated with granites of the Chuya-Kodar complex in the northern part of the Baikal folded region within the Baikal-Patom fold-thrust belt, which is mainly composed of shelfal carbonate-terrigenous sedimentary rocks of the passive southern margin of the Siberian craton (Figure 3). The northern segment of this belt includes a series of uplifts (called Chuya, Tonod, Necher, and Kutim) where Paleoproterozoic intrusive and supracrustal rocks of the folded basement are exposed.

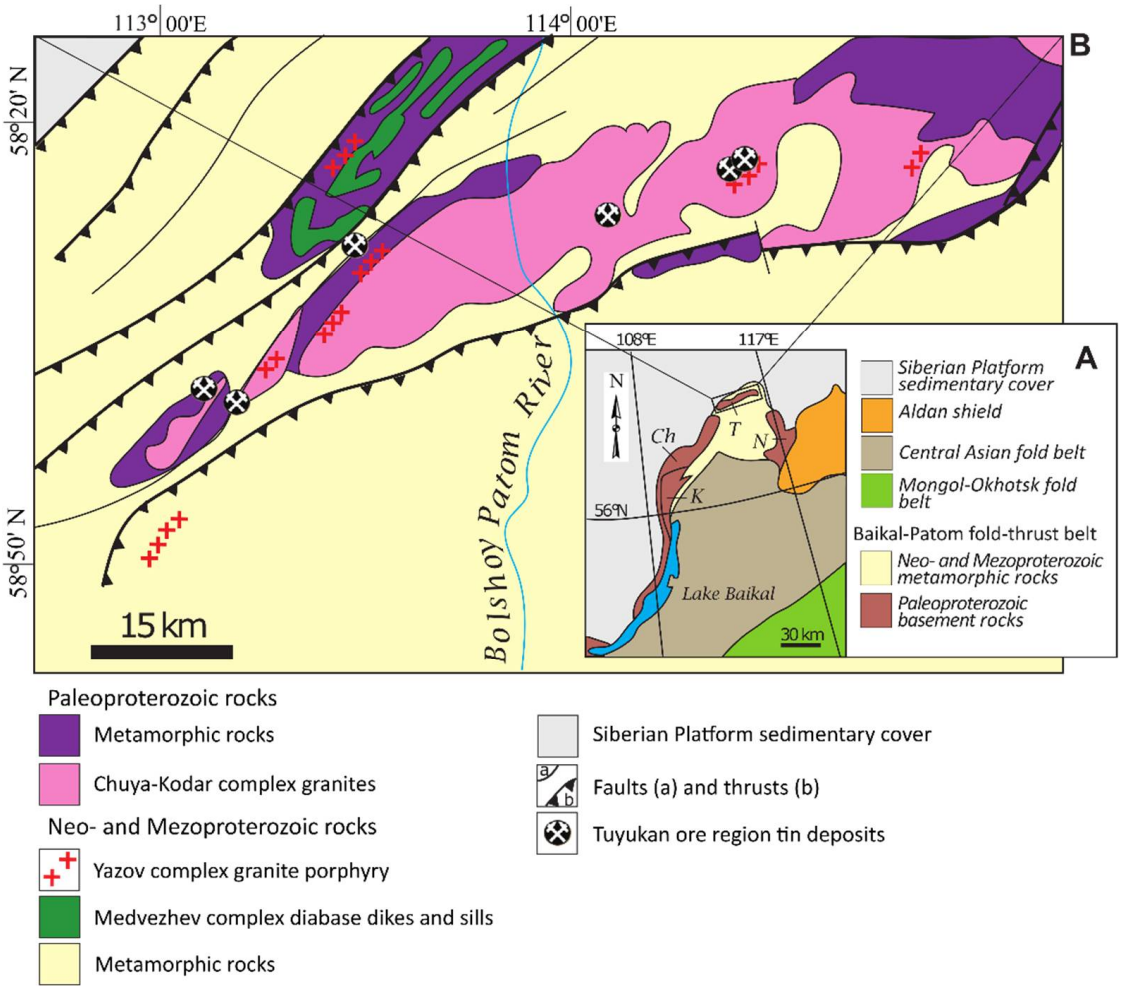

Figure 3. Regional geological map (**A**) and locations of the Yazov and Chuya-Kodar granites and ore metasomatites sampling sites for U-Pb geochronology (**B**) Uplifted Paleoproterozoic rocks: Ch—Chuya uplift, K—Kutim uplift, T—Tonod uplift, and N—Necher uplift. Symbols of the Yazov complex granite porphyry and Tuyukan ore region tin deposits are not to scale (modified from Neymark et al. [16]).

The tin deposits and prospects of the Tuyukan ore region are located within the Tonod uplift. Tin mineralization is related to the Paleoproterozoic coarse-grained post-collision S-type tin-bearing granites of the Chuya-Kodar complex. Tin ore deposits and occurrences are linear stockwork zones with quartz and quartz-muscovite veins, plus veins and linear zones of tourmaline-muscovite-quartz, microcline-muscovite-quartz, albite-quartz, and muscovite-quartz metasomatites with cassiterite mineralization (Figures 2B,C and 3C–H in Neymark et al. [16]). The deposits are confined to the ore-controlling faults of northeastern strike and are associated with small stocks and dikes (sometimes explosive breccias) of the Neoproterozoic Yazov porphyry granite and mainly hosted by the Chuya-Kodar granites. The main ore mineral is cassiterite. The ore also contains subordinate amounts of arsenopyrite, galena, sphalerite, chalcopyrite, and pyrrhotite. Previous dating of the Yazov granites and ores [16,51] confirmed the ~720 Ma age of the granites and rules out any genetic relations between the tin ore dated at ~1850 Ma and the Yazov granites. The geochronological data suggested that the tin ore is related to the older Paleoproterozoic host Chuya-Kodar coarse-grained porphyry two-mica granites dated at 1846 ± 8 Ma [40]. In this paper we use all U-Pb-isotope analyses for cassiterite samples L-304, L-316, L-490, and L-528 from Neymark et al. [16] to construct a combined Pb-Pb isochron to improve the precision of the ore age estimate.

2.3. Pitkäranta Mining District (PMD) Tin-Rare Metal-Base Metal Skarn Deposits

The historic mining district of Pitkäranta in the Ladoga region, Fennoscandian Shield (Figures 1 and 4), was exploited for Fe, Cu, Zn, Pb, Sn, and Ag in the nineteenth and twentieth centuries. It is located on the northeastern shore of Lake Ladoga, NW Russia and extends for ~40 km from north to south at the western edge of the Salmi anorthosite-rapakivi granite batholith and has a maximal width of four to five km. The main type of ore deposits in the region is represented by skarn deposits with a multi-metal Fe, Sn, rare metal, base metal, and fluorite mineralization. The Pitkäranta ores constitute a classical skarn type, formed when granite-related hydrothermal fluids reacted with marble [52]. The deposits are related to the carbonate horizons of the Pitkäranta suite which encloses the gneiss-granite domes. Linear greisen zones carrying Be, Sn, Mo, and Cu mineralization are commonly found within various types of the rapakivi granites and granite gneisses of the domes. Tin was discovered in PMD skarns in 1834 [53,54]. Brief descriptions of the ~1.54 Ga Salmi batholith and Pitkäranta ore field and previous geochronology of granites and ores were published [55–58]. The granites are enriched in a number of rare metals (including Sn) and F. Geochemically they belong to the within-plate A-type granites. Salmi granitoids are strongly differentiated and their later intrusive phases are represented by small bodies and dikes of topaz-bearing granites.

A cassiterite sample, SPG, from the Pitkäranta mining district was dated previously [13,19,20] and was also used as a matrix-matched reference material in LA-ICPMS U-Pb dating to correct for U/Pb instrumental bias [13,15,16,59]. During this study we analyzed five more cassiterite samples from the Pitkäranta region collected at the Old Mine Field (sample of pyroxene-garnet (Px-Gar) skarn 31 and sample LA-1 of quartz-carbonate metasomatite developed over a Px-Gar skarn with coarse-grained cassiterite) and at the Kitilä deposit (samples of Px-Gar-Mt skarns with cassiterite O-4-11, X-146, and VSH-5).

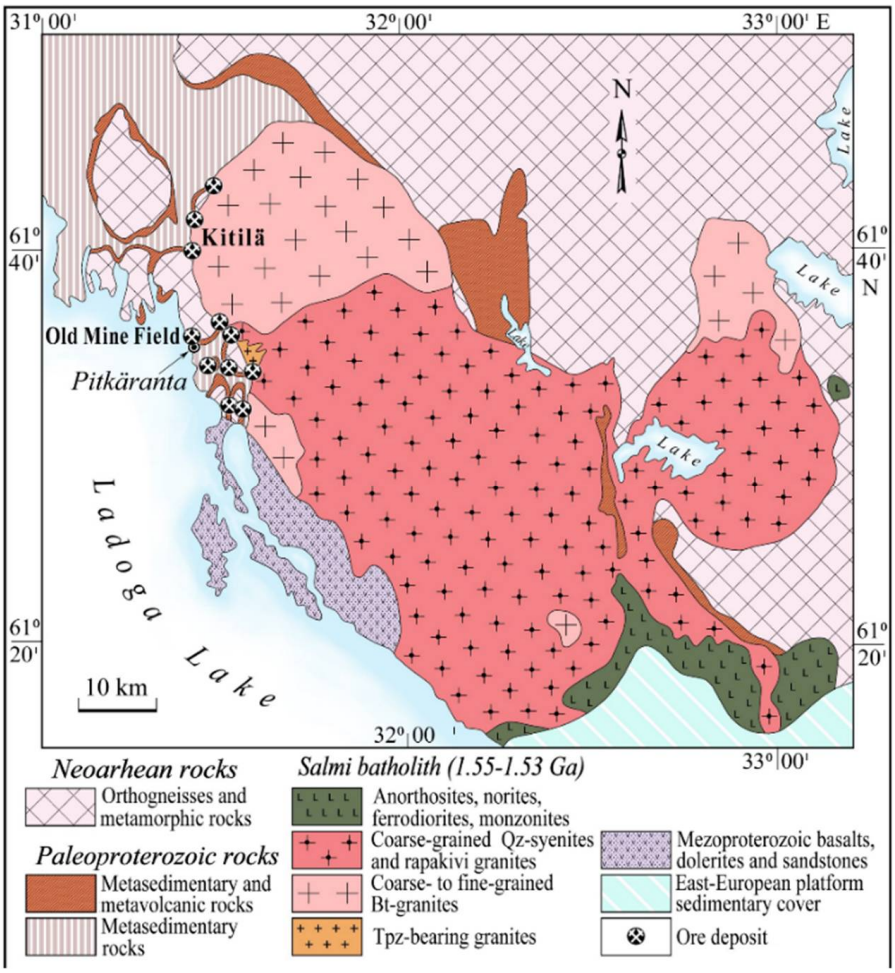

Figure 4. Geologic map of the Pitkäranta mining district, South Karelia, showing locations of skarn deposits. Modified from Amelin et al. [55] and Larin [58]. Bt—biotite; Qz—quartz; Tpz—topaz.

2.4. Mokhovoe Porphyry Tin Deposit

The tin-bearing metasomatites of the Mokhovoe tin deposit are located in western Transbaikalia (in the Muya District of the Republic of Buryatia), in the Baikal-Muya belt of the East-Baikal segment of the Central Asian fold belt (Figure 5), and the Mokhovoe tin deposit is ~370 km south of the tin deposits in the Tonod uplift. This 20 km × 30 km structure is mainly composed of volcanics within the Zhanok suite and by intrusive bodies of Bambukoy granites. The ID-TIMS zircon ages 834 ± 23 Ma and 818 ± 7 Ma [60] for volcanics and granites, respectively, coincide within error. The deposit consists of 10 tubular and two lenticular bodies of magnetite-feldspar metasomatites with cassiterite-chalcopyrite and magnetite-hematite mineralization. The main ore minerals are magnetite, hematite, mushketovite, cassiterite, chalcopyrite, bornite, pyrite, and rare stannite. The ore bodies are hosted by felsic rocks of the Bambukoy igneous complex that have geochemical features similar to those of S-type granites. Tin concentrations in the rocks are elevated (2.7–7.2 ppm Sn) but are not high enough to be classified as tin granites [60].

The age of the tin mineralization is constrained by the presence of magnetite/hematite pebbles with minor cassiterite in basal conglomerates of the Amatkansk suite of the Ediacarian (635–540 Ma) age [60]. During this study, we analyzed two cassiterite samples (S-19-7 and S-23-39) separated from magnetite-feldspar metasomatites of the Mokhovoe deposit.

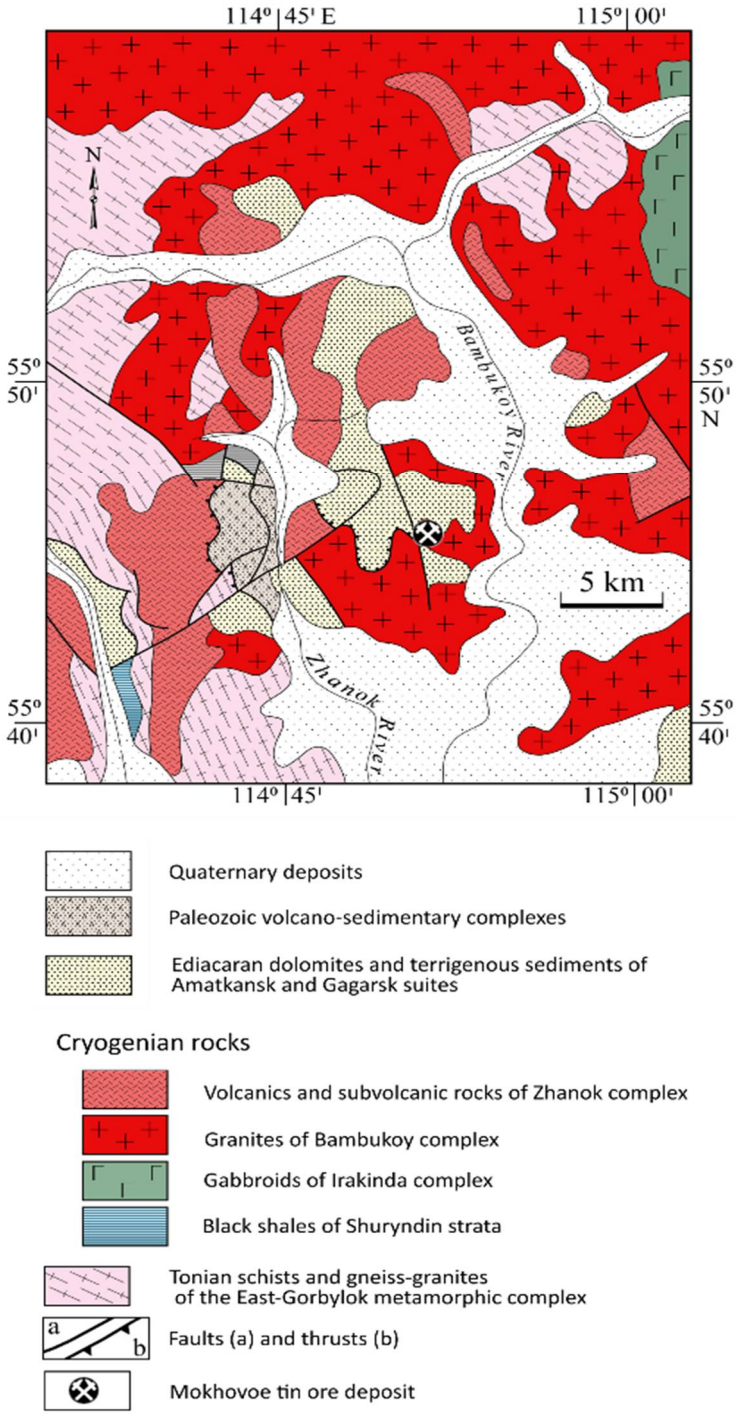

Figure 5. Simplified geologic map of the Mokhovoe tin deposit area, western Transbaikalia, East Siberia (modified from Kozlov et al. [61]).

2.5. Valkumei Silicate-Sulfide Vein Tin Deposit

The significant deposits in Chukotka, Russian Northeast, are at Valkumei (presently being mined), Pyrkakay, Ekug, Telekai, Kukenei, Mramornoe, and Dioritovoe (Figure 6). Most of the known Sn reserves in the region occur in stockworks of the porphyry Sn Pyrkakay deposit [62–64]. The Valkumei Sn silicate-sulfide vein deposit [65] used to serve as the principal source of tin ore for the Soviet Union. It consists of simple and complex veins, mineralized zones, and less common linear stockworks. The deposit occurs mainly within the marginal zone of the Late Cretaceous (108–105 Ma) small post orogenic granitic pluton (Figure 6) and to a lesser degree in Cretaceous sandstone and shale that host the

pluton [30,66]. This pluton belongs to the Chaun igneous complex, composed of quartz monzonites, monzogranites, granites, zinnwaldite granites and ongonites, and topaz-bearing albite-rich microgranites. Mineralization occurs in a north-northwest-trending zone alone the contact of the pluton.

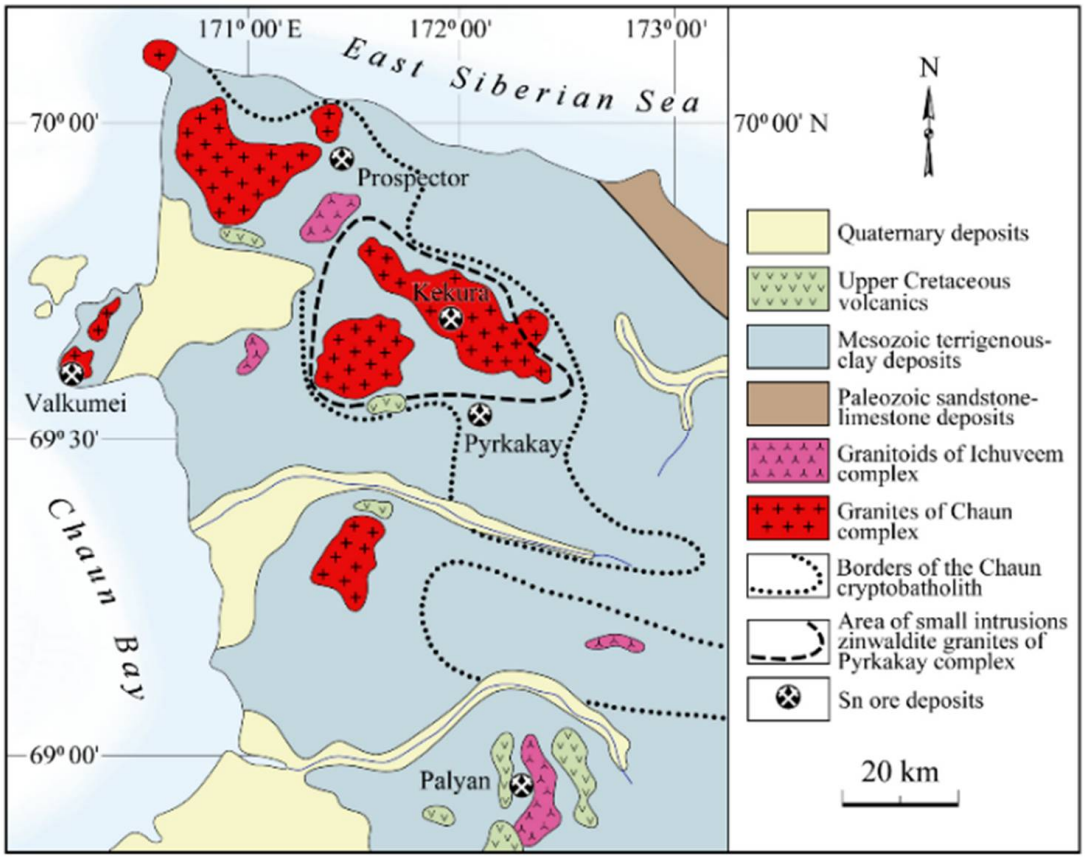

Figure 6. Simplified geologic map showing the distribution of late Mesozoic magmatic bodies and tin ore deposits in Chaun ore district, Chukotka, the Russian Northeast (modified from Alekseev and Alekseev [35]).

The ore bodies commonly consist of a conjugate system of (1) major north-south veins and feathered veinlets, and (2) a zone of approximately east-west- and northwest-trending veins. The deposit hosts 70 minerals; the majority of the veins are composed dominantly of tourmaline with quartz, chlorite, albite, arsenopyrite, cassiterite, pyrrhotite, chalcopyrite, stannite, sphalerite, stibnite, fluorite, and various carbonates. The ore bodies are vertically extensive. The cassiterite-quartz-tourmaline veins are replaced by sulfide veins at depth. The deposit is large, was discovered in 1935, and has been mined from 1941 to the mid-1990s. The average grade is 0.4 to 1.2 percent Sn.

Here, we include data for coarse-grained cassiterite sample W-1 collected from this deposit for in situ U-Pb dating previously reported by Neymark et al. [13].

2.6. Merek Greisen Tin Ore Deposit

The Russian Far East is a part of the Eastern Asia tin belt that extends from Indonesia in the south to the Chukchi Peninsula in the north. The northern part of the Eastern Asia tin belt is represented by five tin ore regions Chukotka, Kolyma, Yana-Indigirka, Khingan-Okhotsk, and Sikhote-Alin [67].

Most deposits are related to Cretaceous and Paleogene tin-bearing volcanic-plutonic complexes localized at an Andean-type transform or active continental margin [68]. The Sn deposits occurring in this belt are typical deposits related to ilmenite-series granitic activities [26,69].

The Merekski ore district (or Dusse-Alin ore district) is located at the eastern margin of the Khanka-Burea massif (Figure 7) and occurs in the eastern contact zone of biotite and/or biotite-muscovite granites of the Dusse-Alin intrusive complex. It is a cassiterite-quartz type containing quartz, muscovite and tourmaline, besides cassiterite, wolframite, molybdenite, and beryl.

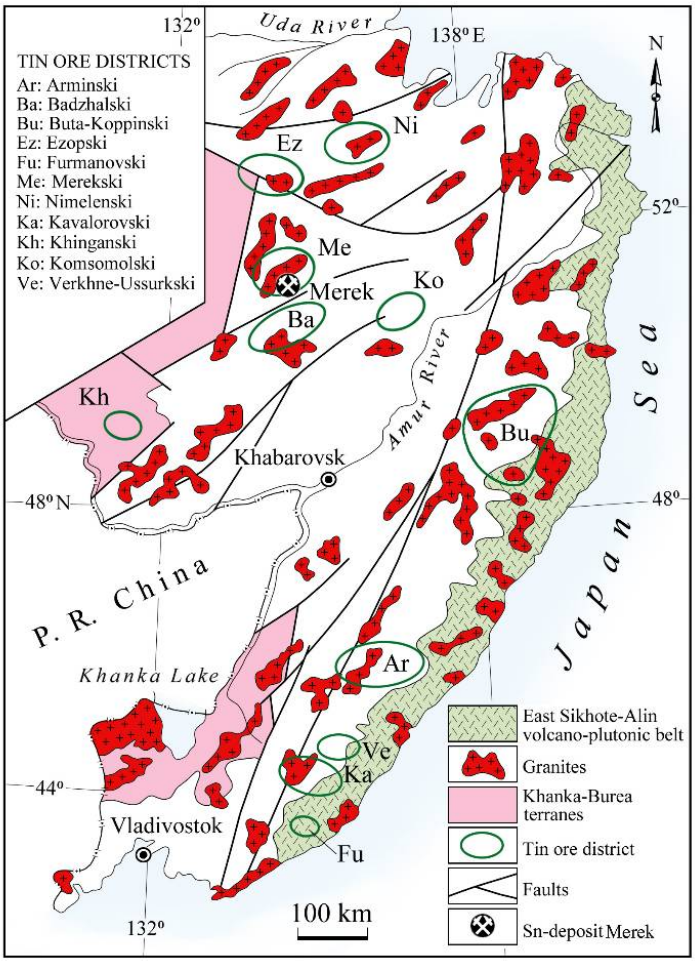

Figure 7. Distribution of Mesozoic intrusive bodies and tin ore districts, the southern Russian Far East (modified from [26]).

About 320 km northeast of the Khinganskoe deposit, muscovite from the mineralized greisen in the biotite and/or biotite-muscovite granite of the Dusse-Alin intrusive complex (90 Ma [69]) within the Merek tin ore deposit was dated by the K-Ar method at 85.9 Ma [26], which is ~4 Ma younger than the host granite itself. We analyzed cassiterite sample MK-1 separated from a mineralized greisen at the Merek deposit.

3. Methods

The rocks were crushed to liberate the cassiterite fragments and crystals prior to handpicking at the Institute of Precambrian Geology and Geochronology (IPGG), St Petersburg, Russia. At the U.S. Geological Survey (USGS), handpicked cassiterite fragments or single large crystals were mounted in epoxy and imaged in transmitted and/or reflected light on a petrographic microscope. Cassiterite is opaque to translucent reddish brown in transmitted light depending on crystallinity and its chemical composition. Internal textures and some inclusions in opaque grains are difficult to identify by light microscope techniques so cathodoluminescence (CL) and backscatter electron (BSE) imaging was used to examine internal characteristics of individual grains. The textural features revealed by

CL primarily originate from the substitution of Ti, Fe, and W for Sn (e.g., [70,71]). Titanium and W behave as luminescence activators and result in light CL features, in contrast to Fe, which quenches luminescence and results in dark features. The images were used to guide our selection of spots for in situ analyses to target inclusion- and fracture/vein-free parts of crystal fragments. Selected CL images of analyzed cassiterite samples are shown in Figure 8.

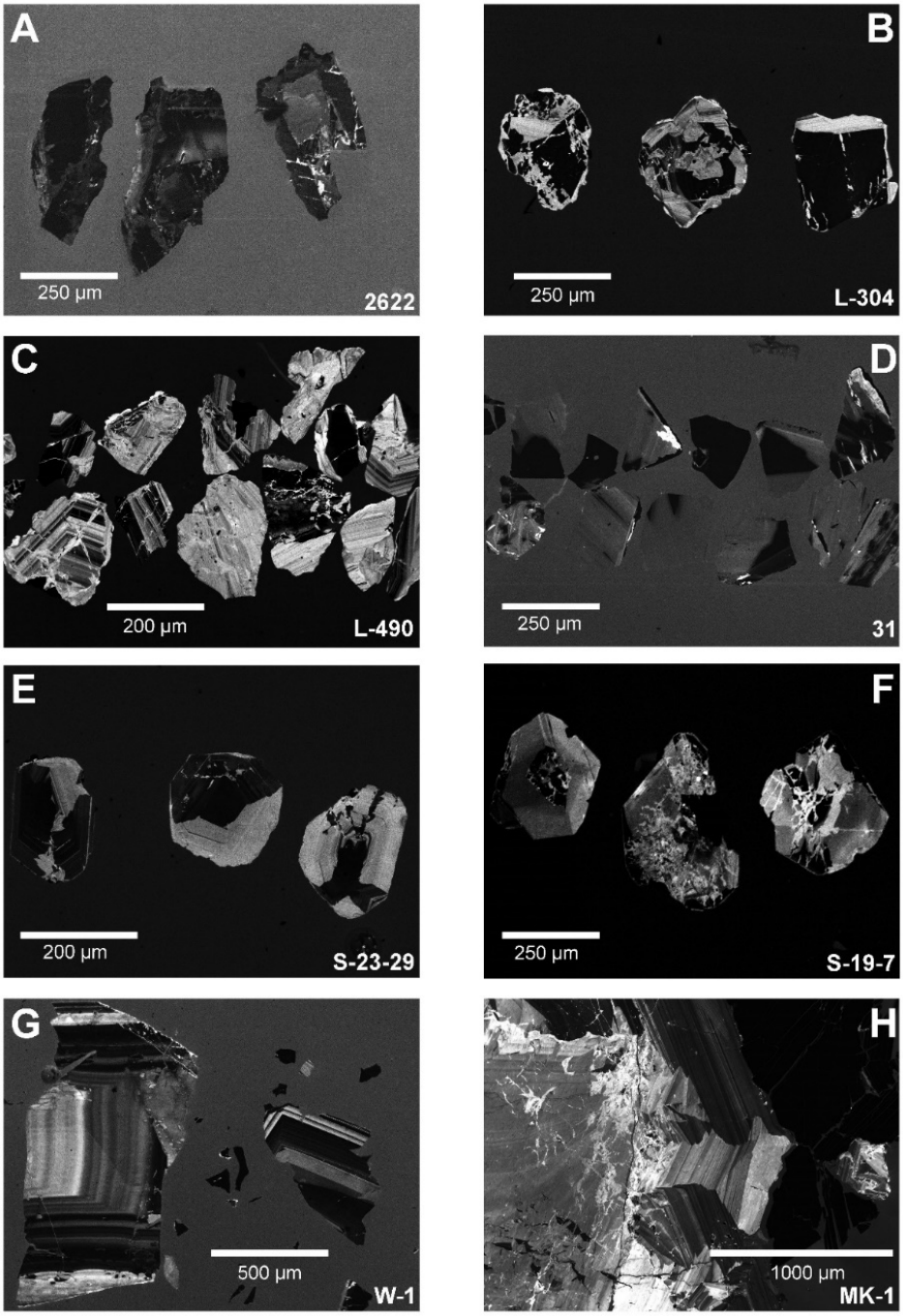

Figure 8. Representative scanning electron microscope (SEM) cathodoluminescence (CL) images of cassiterite grains used for Pb-Pb and U-Pb dating: (**A**) 2622 (East Sayan pegmatite belt, Vishnyakovskoe deposit). CL imaging reveals a combination of both sector and faint oscillatory zoning in

most grains. The oscillatory zoning is commonly at grain margins. Using back-scattered electron and energy-dispersive spectroscopy (BSE-EDS) spot analyses, no mineral inclusions within the cassiterite were found; (**B**) L-304 (Tuyukan ore region, September deposit). The cassiterite exhibits light-colored growth banding in CL interrupted with compositional sector zoning. Minor later staged light-colored veinlets are common throughout. BSE-EDS analyses revealed quartz and plagioclase within the cassiterite matrix; (**C**) L-490 (Tuyukan ore region, Silvery deposit). CL images of the Silvery cassiterite indicate prolific oscillatory zoning with typically fine-scale light-colored banding and coarser-scale dark banding. The grains host inclusions of quartz, apatite, and K-feldspar as discovered with BSE-EDS inspection; (**D**) 31 (Pitkäranta Mining District, Old Mine Field deposit). These grains yielded minimal CL response, although sector zoning throughout the grains and thin, dark, U-rich growths at the crystal margins may be discerned. BSE-EDS evaluation indicate seemingly inclusion-free grains; (**E**) S-23-29 (Western Transbaikalia, Mokhovoe deposit). The cassiterite grains are characterized by extremely fine-scaled zoning, followed by darker sector zoning. BSE-EDS review found no inclusions; (**F**) S-19-7 (Western Transbaikalia, Mokhovoe deposit). CL evidence shows that sector zoning played a dominant role followed by a period of uniformly dark CL activation with sporadic trace element mobility as evidenced by disruptive growth banding in distinct sections of the grains. Inclusions of scheelite and possible clay mineralogy were discovered with BSE-EDS analyses; (**G**) W-1 (Russian Northeast, Valkumei deposit). The Valkumei cassiterite is characterized by distinct oscillatory zoning, commonly with lesser U cores, U-rich mantle areas followed by late-stage U-poor rims. The larger grain at left is showing signs of crystal strain. BSE-EDS examination disclosed inclusion free grains; (**H**) MK-1 (Russian Far East, Merek deposit). This is a small portion of a ~1 cm^2 grain exhibiting sector zoning towards the interior of the grain (at left), followed by fine-scaled oscillatory zoning, and then truncated by a zone of dark or diffuse CL activation (at right). Using BSE-EDS spot analyses, no mineral inclusions within the cassiterite were found.

U-Pb compositions of cassiterite were analyzed at the U.S. Geological Survey (USGS) in Denver, Colorado on a Nu Instruments AttoM ES™ sector field inductively coupled mass spectrometer (SF-ICPMS) coupled to a Teledyne Photon Machines Analyte™ 193 nm ArF excimer laser ablation system with a two-volume HelEx sample cell. Gas flows were optimized in line scan mode on NIST610 for maximum intensity, optimal peak shape, and low oxide production and Th/U fractionation.

Approximate U and Th concentrations (Tables S1 and S2) were obtained using the Iolite™ 2.5 [72] U-Pb geochronology Data Reduction Scheme (U_Pb_Geochronology3) using NIST 612 glass as the primary standard reference material for which U and Th concentrations of ~37.4 and 37.8 ppm, respectively, were certified by the National Institute of Standards (NIST) [73]. NIST glasses can exhibit substantially different elemental fractionation behavior than many common geological matrices, resulting in degraded precision and accuracy for some elements [74,75]. Because of the matrix difference between the NIST 612 soda-lime glass and cassiterite, we assumed the U and Th cassiterite data to be not better than ±20% accurate based on results by Jochum and Stoll [76].

All data were collected with laser spot diameters of between 85–135 μm, a laser repetition rate of 5Hz and laser energy density of between 4.0 and 5.0 J/cm^2. The NIST 612 glass standard was used as a primary non-matrix-matched standard to correct for instrumental Pb-isotope fractionation. A ~1.54 Ga, low-Th, cassiterite sample SPG from a skarn deposit in Russian Karelia was used as a primary matrix-matched reference material to correct for the instrumental U/Pb bias. A ~155 Ma Jian-1 cassiterite from the Jiangxi W-Sn district in the eastern Nanling Range, South China, was used as a secondary matrix-matched reference material to estimate external reproducibility of the LA-ICPMS U-Pb analyses. U-Pb ages for both SPG and Jian-1 samples have been measured by ID-TIMS [19], and our LA-ICPMS data for the SPG sample, presented in Table S1, did not show any statistically significant (beyond two standard deviations, 2 SD uncertainty) deviation from the ID-TIMS results (no systematic error). Replicate analyses (n = 12) of the secondary matrix-matched reference cassiterite Jian-1 show an

external 2 SD reproducibility error of the SPG-normalized $^{206}Pb^*/^{238}U$ lower intercept T-W isochron ages of 1.6% (Table S2).

Methods of the data collection and reduction used in this study were described in detail in Neymark et al. [13]. Our method assumes that there is no matrix effect on the Pb isotope ratios and therefore sample/standard bracketing using matrix-mismatched, well- characterized homogeneous NIST glass standard can be used to correct for the instrumental Pb isotope fractionation. The absence of an appreciable matrix effect on Pb isotopes during the LA-ICPMS analyses was shown in several publications (e.g., [77,78]). We used the Iolite 2.5 output for fractionation-corrected Pb isotope ratios in further offline data reduction. In contrast, the U/Pb ratios for the matrix-matched reference material from the Iolite output are biased from the "true" U/Pb values due to the matrix effect, which is assumed to be the same for the cassiterite reference and unknowns. Then, these biased $^{238}U/^{206}Pb$ ratios and the corrected NIST-normalized $^{207}Pb/^{206}Pb$ ratios from the Iolite output were used to calculate a biased U-Pb age of the matrix-matched reference material using Isoplot V4.15 software [79]. The difference between the biased and known "true" age of the matrix-matched material is used to derive correction factors F for the measured $^{238}U/^{206}Pb$ ratios in unknowns in each analytical session. Finally, these bias-corrected $^{238}U/^{206}Pb$ ratios and $^{207}Pb/^{206}Pb$ ratios from the Iolite were used in Isoplot to calculate Tera-Wasserburg (T-W [80]) $^{238}U/^{206}Pb$-$^{207}Pb/^{206}Pb$ isochron lower intercept ages and ^{207}Pb common Pb-corrected $^{206}Pb^*/^{238}U$ ages assuming Stacey-Kramers model (S-K [81]) Pb_c composition.

The use of the age ratio to determine the correction factor "F" ($F = T_{biased}/T_{true}$, Figure 9A) is not accurate because the age is an exponential function of Pb/U ratios. A proper approach would be to calculate apparent radiogenic $^{238}U/^{206}Pb$ in the standard using the measured LA-ICPMS data and divide it by the $^{238}U/^{206}Pb$ ratio corresponding to the "true" ID-TIMS age of the standard. Chew et al. ([82], Appendix A) proposed to correct within-session bias in the U-Pb ratios by calculating a ratio of the measured lower concordia $^{238}U/^{206}Pb^*$ intercept to that of the true $^{238}U/^{206}Pb^*$ ratio of the standard ($F = R_{b1}/R_{True}$, Figure 9B). However, this method is fully accurate only for geologically young reference materials (<500 Ma) falling in the age range where T-W concordia is reasonably approximated by a horizontal straight line (Figure 9A) and may give biased correction factor estimates for older references where the T-W concordia has a significant curvature (Figure 9B). A more accurate approach was proposed by Roberts et al. [83] who suggested using $F = X_{Rm}/X_{Rc}$ (Figure 9B). This approach, similar to that of Chew et al. [82], requires an assumption about initial $^{207}Pb/^{206}Pb$ in the matrix-matched reference material. If we only use the parameters of its "raw" T-W isochron and the "true" age, the correction factor can be calculated as $F = R_{b2}/R_{True}$ (Figure 9B).

LA-ICPMS results for unknowns are presented in Table S3. All age uncertainties in this paper are given as 2 SD (standard deviations) or 2 SE (standard error = SD/sqrt of the number of values). Uncertainties of U-Pb ages given in parentheses include an added in quadrature external 2 SD reproducibility error of 1.6%. This uncertainty estimate is based on 12 replicates of SPG-normalized U-Pb ages for the Jian-1 secondary matrix-matched reference cassiterite. Uncertainties of Pb-Pb inverse isochron ages for unknowns reported in this paper include an external 2 SD uncertainty of 0.6 percent that was derived from 103 replicate $^{208}Pb/^{206}Pb$ vs. $^{207}Pb/^{206}Pb$ inverse isochron ages of SPG reference cassiterite and added in quadrature to within-run age uncertainty of an unknown. The inverse Pb-Pb isochron approach was also applied to spot analyses in geologically "old" (>500 Ma) unknown samples with spot analyses with $Th/^{206}Pb < 0.01$. The details and limitations of this approach were described in Neymark et al. [13].

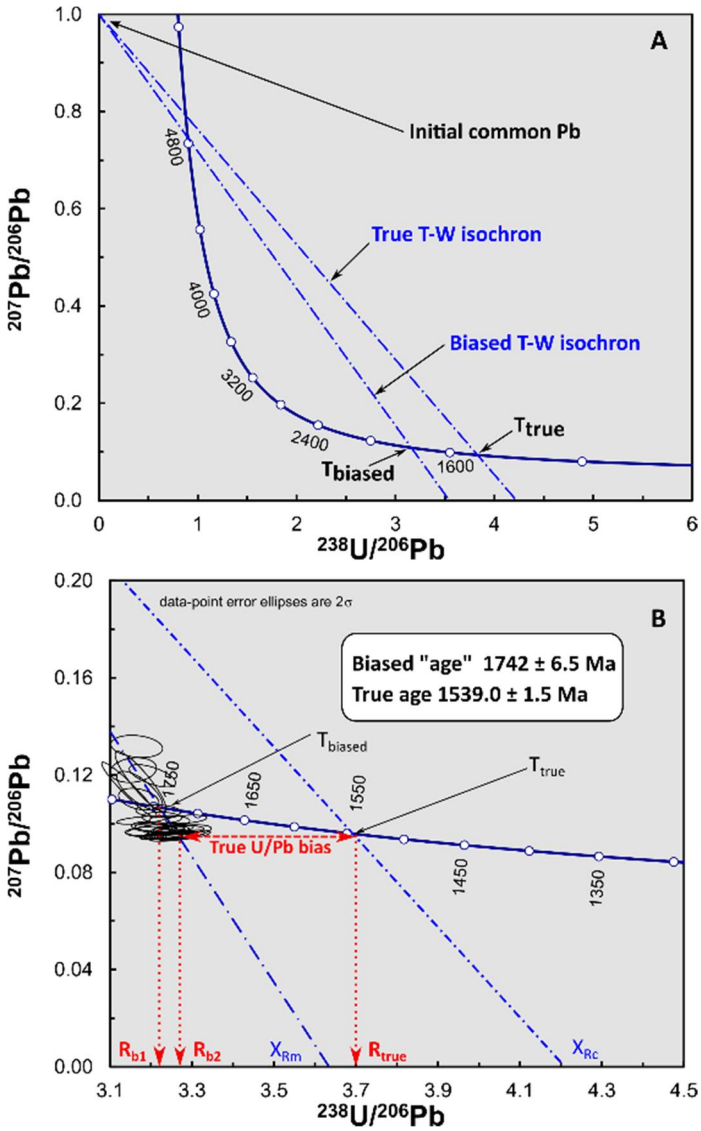

Figure 9. Procedure to determine the correction factor "F" of sample $^{238}U/^{206}Pb$ using the measured array of SPG cassiterite as a reference and assuming no matrix effect for Pb-isotope ratios (**A**). The difference between the true U/Pb bias and the bias calculated from the ratio of ages is shown in (**B**). This figure also shows data (open ellipses) for the SPG reference cassiterite measured in an analytical session.

4. Results

LA-ICPMS results of in situ U-Pb analyses are presented in Table S3. Two plots showing ranges of U and Th concentrations in the samples are also included in that table. The concentrations in cassiterite are highly variable and range from ~0.1 to ~100 ppm and 0 to ~5 ppm for U and Th, respectively.

4.1. Replicate Analyses of the SPG Matrix-Matched Reference Cassiterite

Cassiterite sample SPG from a Px-Gar skarn in Pitkäranta ore district of the Russian Karelia was introduced by Neymark et al. [13] as a matrix-matched reference material for in situ LA-ICPMS U-Pb dating of cassiterite. This coarse-grained cassiterite has elevated U (tens of ppm) and very low Th (<0.01 ppm) contents and is suitable for inverse Pb-Pb isochron dating using ^{208}Pb as a Pb_c proxy. Since then, we have conducted a total of 103 analytical sessions where this cassiterite was used as a matrix-matched reference; a summary of the results is presented in Table S1. An average $^{207}Pb^*/^{206}Pb^*$ (the asterisk

denotes radiogenic Pb component) age value for 103 replicates is 1541.2 ± 9.3 Ma (2 SD). A weighted average age after rejecting five outliers is 1542.05 ± 0.71 Ma (2 SE, MSWD = 1.3). An average initial $^{207}Pb/^{206}Pb$ value from the Y-axis intercepts of T-W isochrons for 82 replicates after rejecting 4 outliers (for sessions with sufficient spread of data points that allowed calculating parameters of T-W isochrons) is 0.92 ± 0.15 (2 SD). A weighted average initial $^{207}Pb/^{206}Pb_c$ value is 0.891 ± 0.011 (2 SE, MSWD = 2.7) in this cassiterite sample.

4.2. Vishnyakovskoe Deposit

Uranium concentrations in 60 spot analyses of cassiterite sample 2622 range from ~0.2 to 39 ppm (median value is 5.8 ppm, Table S3). The U-Pb isotope data are scattered in the T-W Concordia diagram (Figure 10A) thus indicating an open-system behavior and variable initial $^{207}Pb/^{206}Pb$ compositions (from ~0.7 to ~0.95). Selected 17 low $Th/^{206}Pb$ (<0.01) spot analyses define the inverse Pb-Pb isochron age of 1849 ± 20 Ma (Figure 10B). Analyses with radiogenic Pb (measured $^{207}Pb/^{206}Pb$ < 0.16) yield an anchored to Pb_c $^{207}Pb/^{206}Pb$ = 0.95 ± 0.05 T-W isochron lower concordia intercept age of 1833 ± 31 Ma (Figure 10C). A weighted average ^{207}Pb-corrected $^{206}Pb^*/^{238}U$ age (using the S-K Pb_c correction) for 47 spot analyses is 1835 ± 33 Ma (Figure 10D). All three age estimates are within uncertainties of each other. The weighted average U/Pb age was calculated after eliminating nine outliers with younger apparent U-Pb ages which may indicate either radiogenic Pb loss or formation of younger cassiterite generation(s).

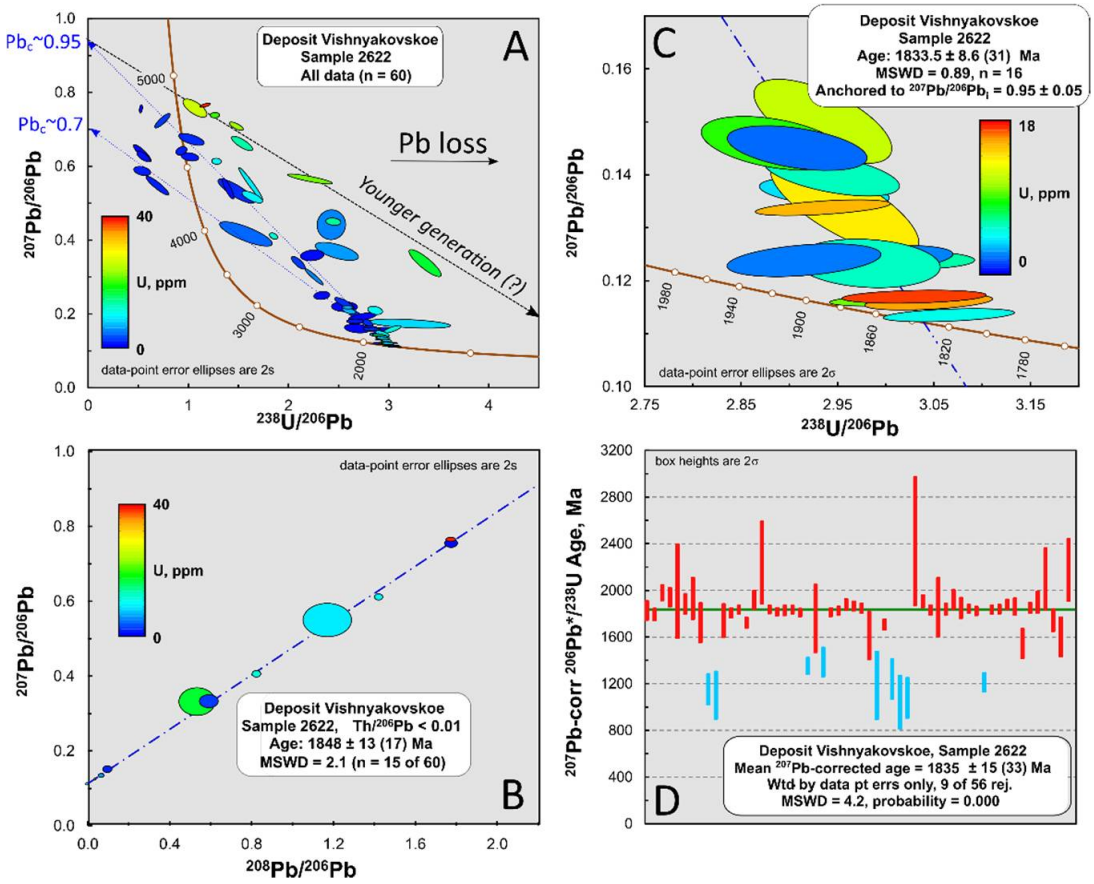

Figure 10. The U-Pb isotope data for a cassiterite sample from the Vishnyakovskoe rare metal deposit, East Sayan. Tera-Wasserburg isochron diagrams for all spot analyses (**A**) and analyses showing the most radiogenic Pb-isotope compositions (**C**). An inverse Pb-Pb isochron (**B**) and a weighted average of the ^{207}Pb-corrected $^{206}Pb^*/^{238}U$ ages (**D**) are also shown. The vertical lines in (**D**) represent age values with 2 standard error (2 SE) bars. The blue lines are outliers not included in the weighted average calculation.

4.3. Tonod Uplift Tin Deposits

Isotope data for the Tonod uplift tin deposits were published in Neymark et al. [16] and combined data for four cassiterite samples (418 spot analyses) are presented here. Uranium concentrations in spot analyses of cassiterite samples L-304, L-316, L-490, and L-528 range from ~0.5 to 57 ppm (median value is 4.4 ppm, Table EA4 in Neymark et al. [16]. Like in the Vishnyakovskoe deposit the U-Pb data are scattered in the T-W diagram (Figure 11A) indicating both potential variability in Pb_c compositions and open U-Pb system behavior. Analyses with lower $Th/^{206}Pb$ ratios (<0.01, n = 93) define an inverse Pb-Pb isochron age of 1861 ± 12 Ma (rounded off age value with an external uncertainty here and hereafter shown in parentheses, Figure 11B). Analyses with radiogenic Pb (measured $^{207}Pb/^{206}Pb$ < 0.13) yield an anchored to Pb_c $^{207}Pb/^{206}Pb$ = 0.95 ± 0.05 T-W isochron lower concordia intercept age of 1846 ± 31 Ma (Figure 11C). The weighted average ^{207}Pb-corrected $^{206}Pb^*/^{238}U$ age (using S-K 1.85 Ga Pb_c correction) for 395 spot analyses is 1631 ± 32 Ma (Figure 11D). This weighted average U/Pb age is younger than the Pb-Pb and lower concordia intercept T-W isochron ages and indicates younger apparent ages for the significant portion of spot analyses due to either radiogenic Pb loss or formation of younger cassiterite generation(s).

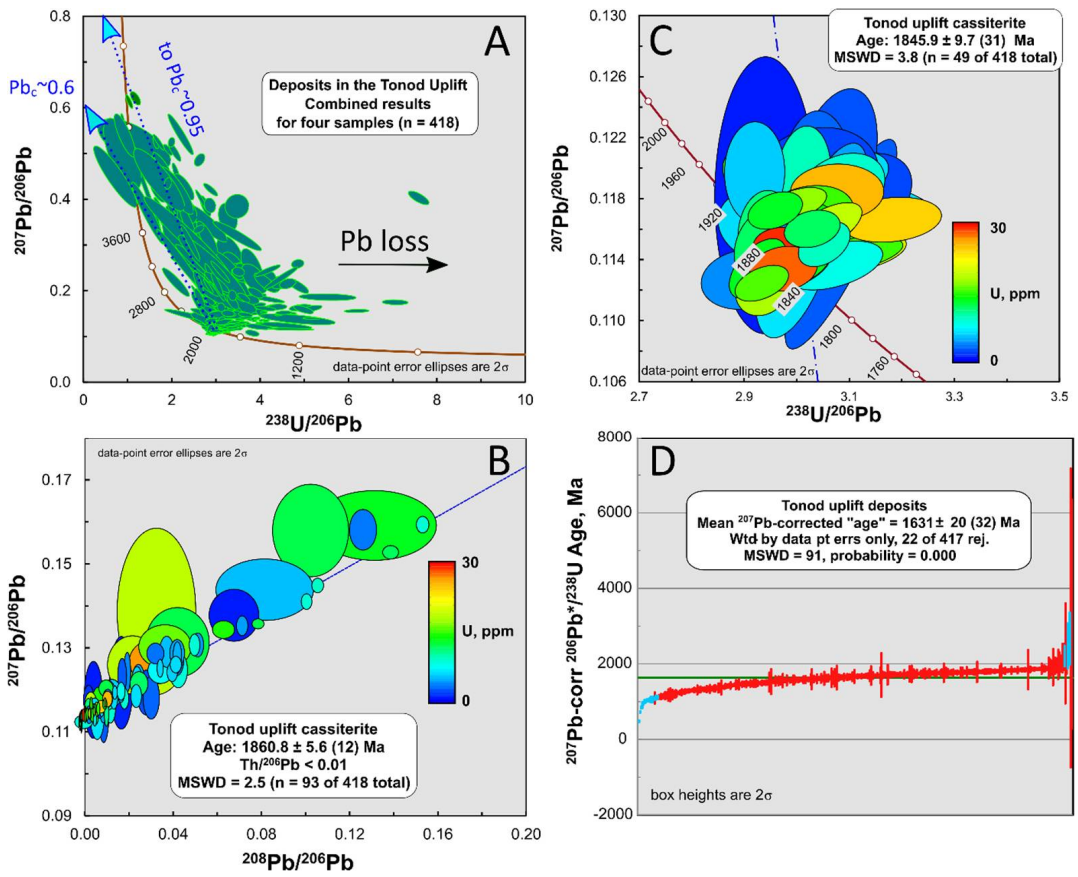

Figure 11. The U-Pb isotope data for cassiterite samples from the Tonod uplift (Tuyukan ore region), Baikal folded region. Tera-Wasserburg isochron diagrams for all spot analyses (**A**) and analyses showing the most radiogenic Pb-isotope compositions (**C**). An inverse Pb-Pb isochron (**B**) and a weighted average of the ^{207}Pb-corrected $^{206}Pb^*/^{238}U$ ages (**D**) are also shown. The vertical lines in (**D**) represent age values with 2 standard error (2 SE) bars. The blue lines are outliers not included in the weighted average calculation.

4.4. Pitkäranta Mining District Skarn Deposits

LA-ICPMS U-Pb data for the coarse-grained cassiterite sample SPG collected from a Px-Gar skarn were presented in Neymark et al. [13]; here we report data for five more cassiterite samples from that ore district (Table S3).

Low-Th (median 4.8 × 10^{-4} ppm Th) cassiterite sample 31 from a Px-Gar skarn in the Old Mine Field has highly variable U concentrations of ~0.2 to ~59 ppm (median value of 9.1 ppm U). This sample yielded T-W isochron, inverse Pb-Pb isochron, and weighted average ^{207}Pb-corrected ages of 1543.3 ± 25 Ma, 1543.4 ± 11 Ma, and 1536 ± 28 Ma, respectively (Figure 12A–C).

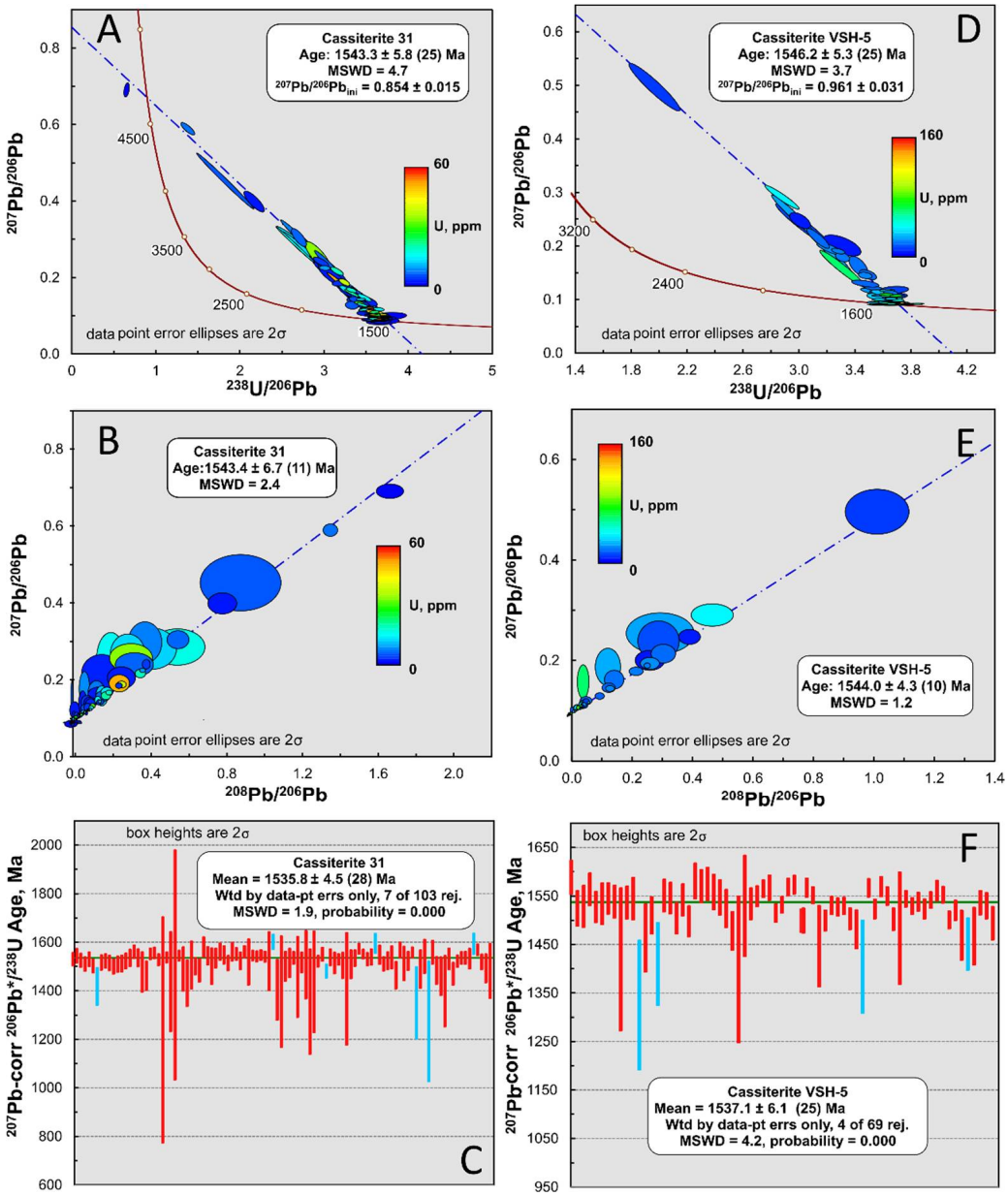

Figure 12. The U-Pb isotope data for cassiterite samples 31 (**A**–**C**) and VSH-5 (**D**–**F**) from the Pitkäranta Mining District skarn deposits. Tera-Wasserburg isochron diagrams (**A**,**D**), inverse Pb-Pb isochrons (**B**,**E**) and weighted averages of the ^{207}Pb-corrected ^{206}Pb*/^{238}U ages (**C**,**F**) are also shown. The vertical lines in (**C**,**F**) represent age values with 2 standard error (2 SE) bars. The blue lines are outliers not included in the weighted average calculation.

The Cassiterite sample VSH-5 from a Px-Gar-Mt skarn (Kitilä deposit) is slightly higher in Th (median 1.7 × 10^{-2} ppm Th) and is generally higher in U (median value of 28.3 ppm U). This sample yielded T-W isochron, inverse Pb-Pb isochron, and weighted average ^{207}Pb-corrected ages of 1546 ± 25 Ma, 1544.0 ± 10 Ma, and 1537 ± 29 Ma, respectively Figure 12D–F).

Cassiterite sample O-4-11 also separated from a Px-Gar-Mt skarn (Kitilä deposit) is slightly higher in U (median value of 32.2 ppm U). This cassiterite yielded T-W isochron, inverse Pb-Pb isochron, and weighted average ^{207}Pb-corrected ages of 1543.9 ± 25 Ma, 1542 ± 1 3 Ma, and 1544 ± 25 Ma, respectively Figure 13A–C).

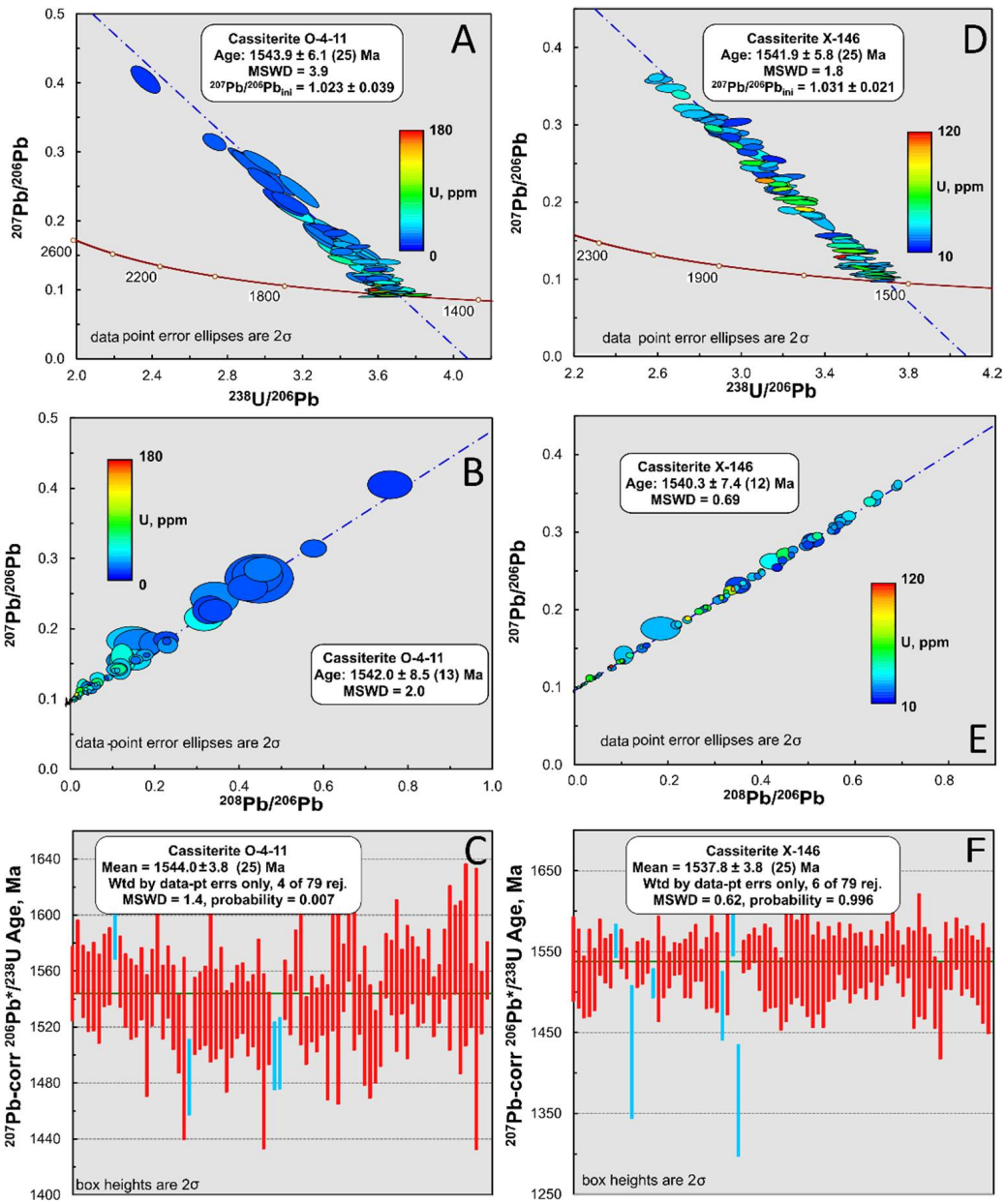

Figure 13. The U-Pb isotope data for cassiterite samples O-4-11 (**A**–**C**) and X-146 (**D**–**F**) from the Pitkäranta Mining District skarn deposits. Tera-Wasserburg isochron diagrams (**A**,**D**), inverse Pb-Pb isochrons (**B**,**E**) and weighted averages of the ^{207}Pb-corrected ^{206}Pb*/^{238}U ages (**C**,**F**) are also shown. The vertical lines in (**C**,**F**) represent age values with 2 standard error (2 SE) bars. The blue lines are outliers not included in the weighted average calculation.

Another cassiterite sample X-148 from the Kitilä deposit Px-Gar-Mt skarn is slightly higher in Th (median value of 0.63 ppm Th) and has U concentration (median value 28.8 ppm U) similar to other samples. This sample yielded T-W isochron, inverse Pb-Pb isochron, and weighted average ^{207}Pb-corrected ages of 1542 ± 25 Ma, 1540 ± 12 Ma, and 1538 ± 25 Ma, respectively (Figure 13D–F).

A coarse-grained cassiterite sample LA-1 separated from a quartz-carbonate metasomatite developed over a Px-Gar skarn (Old Mine Field) has much lower U concentration

(median value 2 ppm U) and moderate Th (median 0.21 ppm Th). Lower U content in this sample results in most Th/^{206}Pb ratios of > 0.01. These values are too high and do not allow the usage of ^{208}Pb as a Pb$_c$ proxy in ^{208}Pb/^{206}Pb-^{207}Pb/^{206}Pb inverse Pb-Pb isochrons (see Neymark et al. [13] for the discussion). This sample yielded T-W isochron and weighted average ^{207}Pb-corrected ages of 1551 ± 28 Ma and 1546 ± 26 Ma, respectively Figure 14A,B).

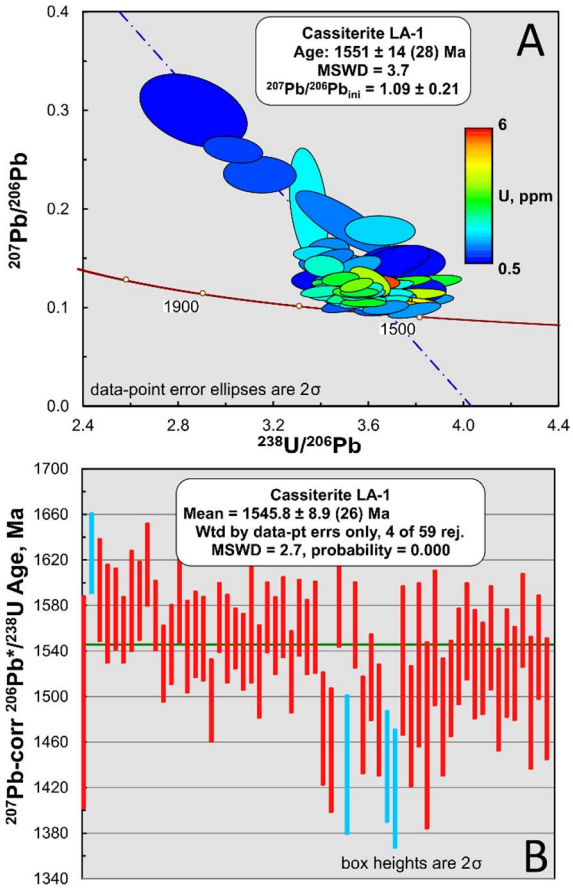

Figure 14. The U-Pb isotope data for cassiterite sample LA-1 from the Pitkäranta Mining District skarn deposit. Tera-Wasserburg isochron diagram and a weighted average of the ^{207}Pb-corrected ^{206}Pb*/^{238}U ages are shown in (**A**,**B**), respectively. The vertical lines in (**B**) represent age values with 2 standard error (2 SE) bars. The blue lines are outliers not included in the weighted average calculation.

4.5. Mokhovoe Deposit

Two samples of cassiterite separated from tin-bearing metasomatites have moderate U concentrations (median U 11.8 and 20.3 ppm in samples S-13-39 and S-19-7, respectively, Table S3). Data for both samples are scattered on the T-W diagrams (Figure 15A,E) which may indicate open-system behavior and variable Pb$_c$ compositions.

Spot analyses of sample S-23-39 with most radiogenic Pb (n = 14, Figure 15B) define an anchored T-W isochron with lower-intercept age of 809 ± 13 Ma. A similar age of 813 ± 14 Ma is obtained for this sample from an inverse Pb-Pb isochron for selected 28 spot analyses with lower Th/^{206}Pb ratios (Figure 15C). A weighted average ^{207}Pb-corrected U-Pb age is 811 ± 17 Ma (Figure 15D).

Spot analyses of sample S-19-7 with most radiogenic Pb (n = 16, Figure 15G) define an anchored T-W isochron with lower-intercept age of 813 ± 21 Ma. A similar, within error age of 821 ± 27 Ma is obtained for this sample from an inverse Pb-Pb isochron for selected 28 spot analyses with lower Th/^{206}Pb ratios of <0.01 (Figure 15F). A weighted average ^{207}Pb-corrected U-Pb age of this sample is 798 ± 19 Ma (Figure 15H).

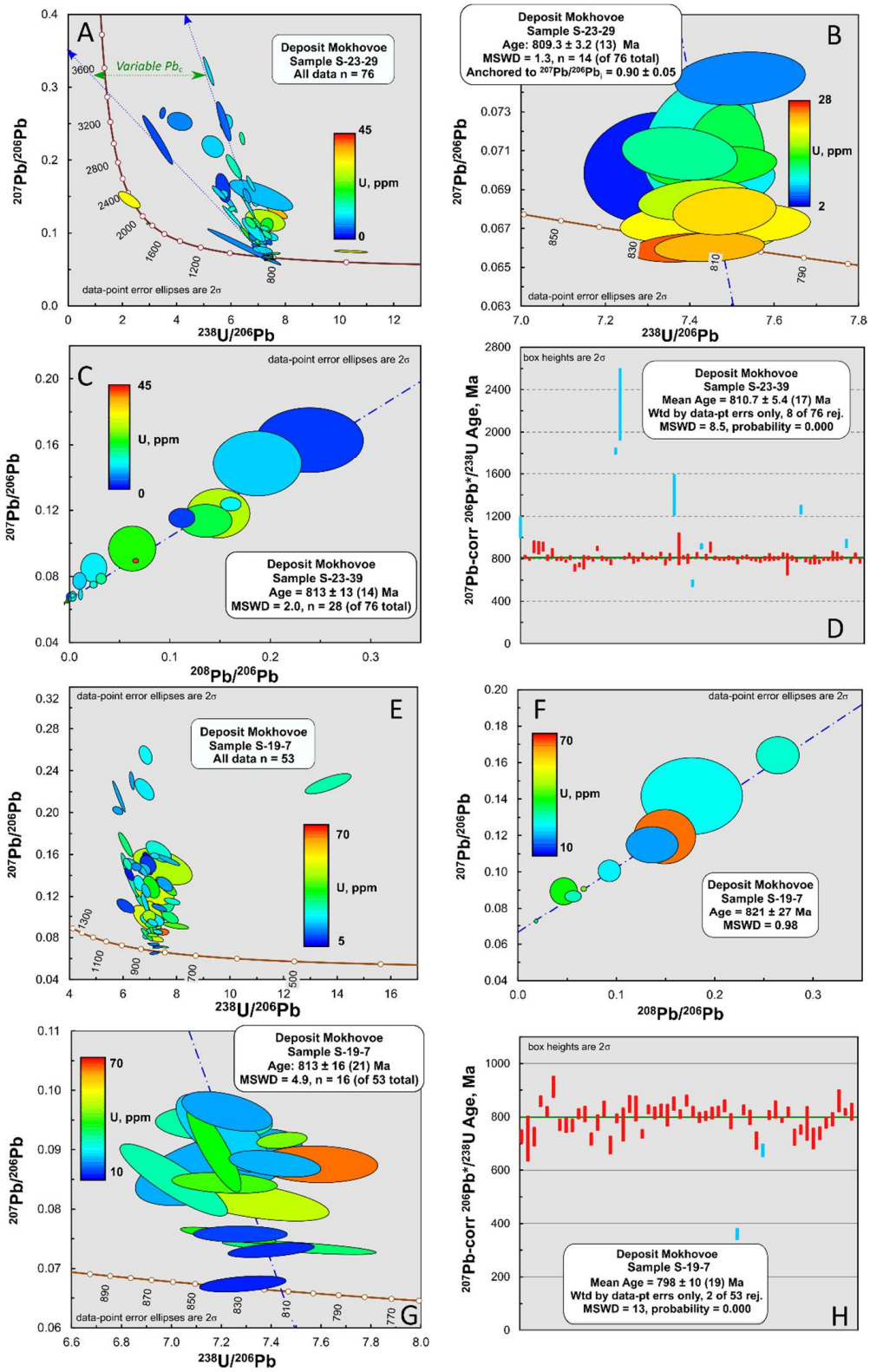

Figure 15. The U-Pb isotope data for cassiterite samples S-23-39 (**A**–**D**) and S-19-7 (**E**–**H**) from the Mokhovoe deposit. Tera-Wasserburg isochron diagrams (**A**,**B**,**E**,**G**), inverse Pb-Pb isochrons (**C**,**F**) and weighted averages of the ^{207}Pb-corrected ^{206}Pb*/^{238}U ages (**D**,**H**) are also shown. The vertical lines in (**D**,**H**) represent age values with 2 standard error (2 SE) bars. The blue lines are outliers not included in the weighted average calculation.

4.6. Valkumei Deposit

Spot analyses of sample W-1 (n = 119, median U 17 ppm, data from Neymark et al. [13] form a T-W isochron (Figure 16A) defining a lower-intercept age of 108.4 ± 2.2 Ma and a Y-axis intercept initial $^{207}Pb/^{206}Pb$ value of 0.840 ± 0.017. This initial $^{207}Pb/^{206}Pb$ value is within error of the S-K model value and the anchored T-W isochron age is 108.5 ± 1.7 Ma (Figure 16B). A ^{207}Pb-corrected age is 108.3 ± 2.2 Ma (Figure 16C). The large number of analyses for this sample was needed because very low U of 0.37 ppm in some spots resulted in elevated errors of the measured U/Pb ratios. The cassiterite age is similar to the age of the Cretaceous (108–105 Ma) Pevek granite-adamellite-granodiorite pluton [30,84] that is spatially associated with the deposit. An attempt to apply an inverse $^{208}Pb/^{206}Pb$-$^{207}Pb/^{206}Pb$ isochron to 45 spot analyses with $Th/^{206}Pb$ < 0.01 (not shown) resulted in an imprecise age estimate of 117 ± 39 Ma. This result confirms a limited applicability of Pb-Pb dating to Mesozoic cassiterite samples.

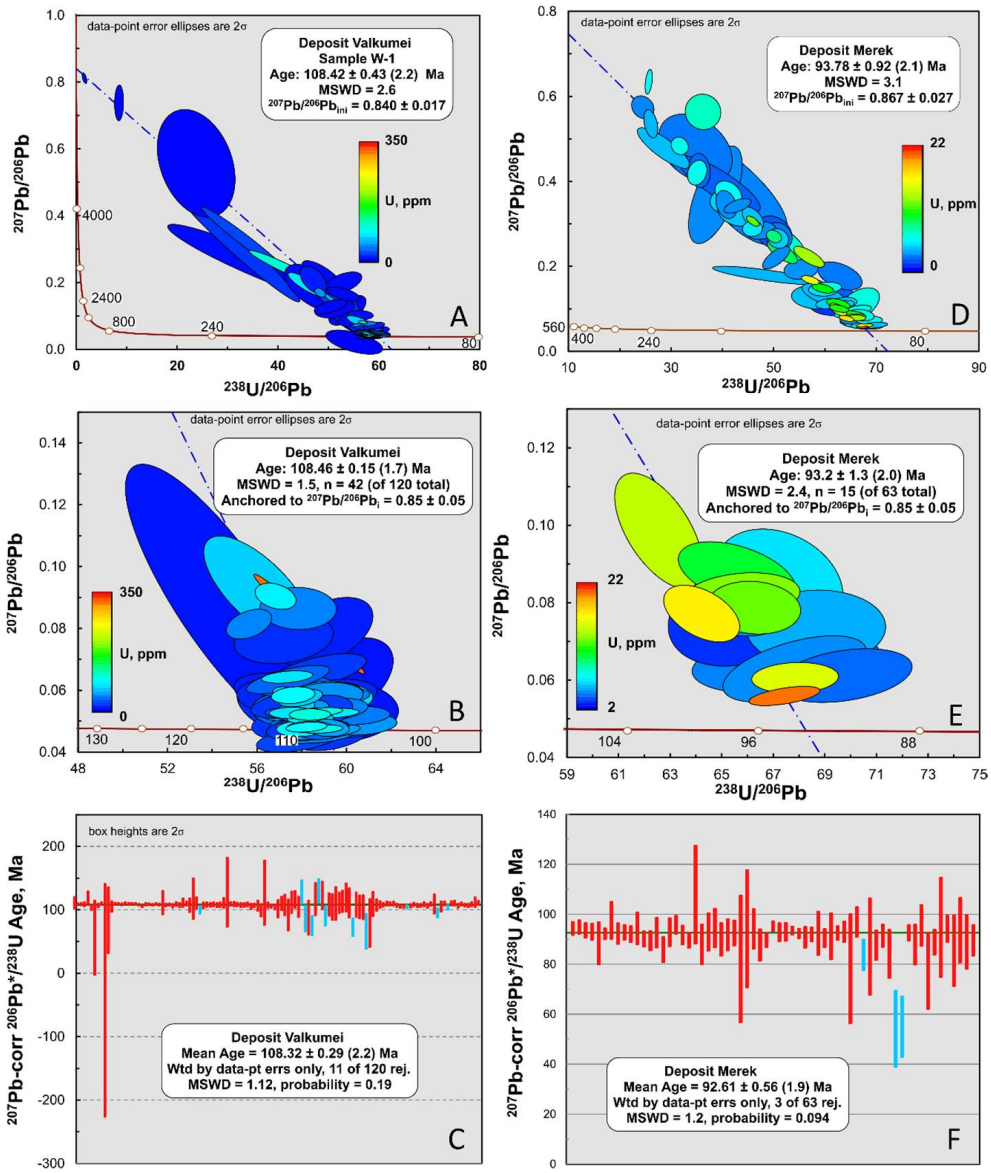

Figure 16. The U-Pb isotope data for cassiterite samples W-1 (**A**–**C**) and MK-1 (**D**–**F**) from the Valkumei and Merek deposits. Tera-Wasserburg isochron diagrams (**A**,**B**,**D**,**E**) and weighted averages of the ^{207}Pb-corrected $^{206}Pb^*/^{238}U$ ages (**C**,**F**) are also shown. The vertical lines in (**C**,**F**) represent age values with 2 standard error (2 SE) bars. The blue lines are outliers not included in the weighted average calculation.

4.7. Merek Deposit

Spot analyses of cassiterite sample MK-1 separated from a tin-mineralized greisen (n = 63, median U of 4.2 ppm) form a T-W isochron corresponding to a lower intercept age of 93.8 ± 2.1 Ma and initial $^{207}Pb/^{206}Pb$ ratio of 0.867 ± 0.027 (Figure 16D). An anchored T-W isochron yields a similar age of 93.2 ± 2.0 Ma and a weighted average ^{207}Pb-corrected U-Pb age of this sample is 92.6 ± 1.9Ma (Figure 16E,F). No attempt was undertaken to apply an inverse $^{208}Pb/^{206}Pb$-$^{207}Pb/^{206}Pb$ isochron to the data because only one spot analysis yielded $Th/^{206}Pb < 0.01$.

5. Discussion

5.1. A Problem of Heterogeneous Isotopic Composition of Initial Pb in Cassiterite

Tapster and Bright [19] reported a high-precision ID-TIMS ~285 Ma U-Pb age for cassiterite from the Cligga Head granite (Cornwall, UK). They interpreted their results as strongly suggesting variable Pb_c isotopic composition and concluded that a simple binary mixture between a radiogenic and Pb_c may not be expected within and between crystals. These authors postulated that some of the overdispersion on T-W isochron diagrams presented in Neymark et al. [13] could be attributed to variable Pb_c isotopic compositions within cassiterite that are inherited from the hydrothermal systems. They also claimed that this complexity in the U-Pb systematics represents a potential limitation on the accuracy of the resulting age interpretation of cassiterite. This over-dispersion on T-W isochron diagrams based on LA-ICPMS data may be masked by low precision of individual data points but may bias the regression of a dataset away from the accurate lower intercept with concordia.

We tested this suggestion using replicate analyses of our SPG reference cassiterite (Table S1) and assumed that a variable isotopic composition of Pb_c should cause some excess scatter of the results obtained in different analytical sessions. We indeed observed an excess scatter (MSWD = 2.7, Table S1) which is statistically significant beyond uncertainty for n = 82. Also, the SPG initial $^{207}Pb/^{206}Pb$ weighted average value of 0.891 ± 0.011 (2 SE) is significantly lower than the $^{207}Pb/^{206}Pb$ value of 1.004 ± 0.014 (2 SD, n = 30) in acid-leached feldspars from the Salmi granites that are considered to be genetically linked with the skarn mineralization [56]. It is also lower than the average value of 1.0104 ± 0.0062 (2 SD, n = 11) in galena from the skarns [25]. Additional cassiterite analyses for five samples from skarns in the Pitkäranta mining district also yielded variable estimates of $^{207}Pb/^{206}Pb_c$ values of 0.854 ± 0.15, 0.961 ± 0.031, 1.023 ± 0.039, 1.031 ± 0.021, and 1.09 ± 0.21 derived from Y-axis intercepts of unconstrained T-W isochrons (Figures 12–14). Scattered data points on the T-W concordia diagrams for cassiterite samples from the Vishnyakovskoe deposit (Figure 10A), deposits within the Tonod uplift (Figure 11A), and the Mokhovoe deposit (Figure 15A) may also indicate variable Pb_c compositions in these samples.

The data indicate that Pb_c in low-Pb cassiterite may be a mixture of Pb from a granite-derived fluid and Pb present in situ in the host rocks. Incomplete mixing between the two Pb components during cassiterite formation may potentially cause excess scatter of U-Pb data on T-W isochron diagrams and result in biased lower concordia intercepts as suggested in [19]. One way to minimize the impact of the Pb_c variability for age calculations is to use anchored T-W isochrons based on spot analyses showing the most radiogenic Pb isotope compositions. In this case, anchoring to the S-K model Pb_c composition would not produce any appreciable age bias because the data points plot close to those of concordia.

The ID-TIMS data from Tapster and Bright [19] also allow calculation of a three-point inverse $^{204}Pb/^{206}Pb$-$^{207}Pb/^{206}Pb$ isochron age of 1540.9 ± 3.6 Ma age for the SPG cassiterite, which is within uncertainty with a weighted average of 1542.13 ± 0.76 Ma (2 SE) based on our replicate LA-ICPMS $^{208}Pb/^{206}Pb$-$^{207}Pb/^{206}Pb$ inverse isochron ages (Table S1). Although our LA-ICPMS Pb-Pb age is within error with the ID-TIMS results, it is older than the reported ID-TIMS U-Pb ages of 1536.6 ± 1.0 Ma [19] and 1539.5 ± 0.9 Ma [20]. These two reported U-Pb age values are based on three and two data points, respectively, and are different beyond the error limits. The small number of high-precision ID-TIMS

analyses does not allow us to estimate a potential "geological" scatter of the data points and emphasizes the necessity for better characterization of potential matrix-matched reference materials for in situ cassiterite U-Pb analyses.

5.2. Summary of Cassiterite LA-ICPMS U-Pb Ages

A compilation of U and Th concentrations and U-Pb ages of cassiterite from several ore deposits in Russia, determined by in situ LA-ICPMS, is presented in Table 1. During this work we analyzed nine new samples from five ore deposits located in different parts of Russia from the Baltic Shield in the west to the Far East. All these new samples showed a wide range of U concentrations (ppm to tens of ppm U, similar to previously published data also included in Table 1) and variable degrees of Pb_c concentrations; nonetheless, all were datable by the in situ LA-ICPMS method.

Table 1. Summary of cassiterite U-Pb and Pb-Pb ages determined by in situ LA-ICPMS method.

Mining District/ Ore Deposit	Sample ID	Sample Coordinates	Median U, ppm	Median Th, ppm	Age Type	Age, Ma	±2 SE, Ma	Reference
East Sayan RareMetal Pegmatites,	2622	55°13′02″ N	5.8	4.70×10^{-2}	T-W isochron lower intercept	1833.5	31	This work
Vishnyakovskoe ore deposit		97°43′00″ E			$^{208}Pb/^{206}Pb$-$^{207}Pb/^{206}Pb$ isochron	1848	13	This work
					^{207}Pb-corr wt. av. ^{206}Pb-^{238}U	1835	33	This work
Tonod Uplift, Tuyukan ore district	L-304	59°14′03″ N	4.8	6.1×10^{-1}	Combined four samples T-W isochron lower intercept	1846	31	Data from Neymark et al., 2021 [16]
Ore occurence September	L-316	114°06′02″ E	4.6	4.5×10^{-1}				
Tonod Uplift, Tuyukan ore district, Ore occurrence Silvery	L-490	59°17′03″ N	4.0	8.4×10^{-2}	Combined four samples $^{208}Pb/^{206}Pb$-$^{207}Pb/^{206}Pb$ isochron	1861	12	
	L-528	114°25′02″ E	5.2	1.6×10^{-2}				
Pitkäranta Mining district Old Mine Field	SPG-IV	61°34′46″ N, 31°27′40″ E	29	2.1×10^{-3}	$^{208}Pb/^{206}Pb$-$^{207}Pb/^{206}Pb$ isochron	1543.2	11	Data from Neymark et al., 2018 [13], $n = 782$
Pitkäranta Mining district	31	61°34′46″ N	9.1	4.8×10^{-4}	T-W isochron lower intercept	1543	25	This work
Old Mine Field		31°27′40″ E			$^{208}Pb/^{206}Pb$-$^{207}Pb/^{206}Pb$ isochron	1543.4	11	This work
					^{207}Pb-corr wt. av. ^{206}Pb-^{238}U	1536	25	This work
Pitkäranta Mining district	VSH-5	61°34′46″ N	28	1.7×10^{-2}	T-W isochron lower intercept	1546	25	This work
Old Mine Field		31°27′40″ E			$^{208}Pb/^{206}Pb$-$^{207}Pb/^{206}Pb$ isochron	1544	10	This work
					^{207}Pb-corr wt. av. ^{206}Pb-^{238}U	1537	25	This work
Pitkäranta Mining district	LA-1	61°34′46″ N	2.0	2.1×10^{-1}	T-W isochron lower intercept	1551	28	This work
Old Mine Field		31°27′40″ E			$^{208}Pb/^{206}Pb$-$^{207}Pb/^{206}Pb$ isochron	n.a.	n.a.	This work
					^{207}Pb-corr wt. av. ^{206}Pb-^{238}U	1546	26	This work
Pitkäranta Mining district	O-4-11	61°40′45″ N	32	6.7×10^{-2}	T-W isochron lower intercept	1544	25	This work
Deposit Kitelä		31°26′30″ E			$^{208}Pb/^{206}Pb$-$^{207}Pb/^{206}Pb$ isochron	1542	13	This work
					^{207}Pb-corr wt. av. ^{206}Pb-^{238}U	1544	25	This work
Pitkäranta Mining district	X-146	61°40′45″ N	29	6.3×10^{-1}	T-W isochron lower intercept	1542	25	This work
Deposit Kitelä		31°26′30″ E			$^{208}Pb/^{206}Pb$-$^{207}Pb/^{206}Pb$ isochron	1540	12	This work
					^{207}Pb-corr wt. av. ^{206}Pb-^{238}U	1538	25	This work

Table 1. *Cont.*

Mining District/ Ore Deposit	Sample ID	Sample Coordinates	Median U, ppm	Median Th, ppm	Age Type	Age, Ma	±2 SE, Ma	Reference
Muya District	S-23-29	55°47′53″ N	12	2.9×10^{-2}	T-W isochron lower intercept	809	13	This work
Mokhovoe deposit		114°49′41″ E			$^{208}Pb/^{206}Pb$-$^{207}Pb/^{206}Pb$ isochron	813	13	This work
					^{207}Pb-corr wt. av. ^{206}Pb-^{238}U	811	17	This work
Muya District	S-19-7	55°47′53″ N	20	3.2×10^{-2}	T-W isochron lower intercept	813	21	This work
Mokhovoe deposit		114°49′41″ E			$^{208}Pb/^{206}Pb$-$^{207}Pb/^{206}Pb$ isochron	821	27	This work
					^{207}Pb-corr wt. av. ^{206}Pb-^{238}U	798	19	This work
Russian North East	W-1	69°35′56″ N	17	1.7×10^{-3}	T-W isochron lower intercept	108.4	2.2	Neymark et al., 2018 [13]
Valkumei deposit		170°09′56″ E			^{207}Pb-corr wt. av. ^{206}Pb-^{238}U	108.3	2.2	
Russian Far East	MK-1	51°19′02″ N	4.2	3.7×10^{-2}	T-W isochron lower intercept	93.8	2.1	This work
Merek deposit		134°43′05″ E			^{207}Pb-corr wt. av. ^{206}Pb-^{238}U	92.6	1.9	This work

Older Paleoproterozoic samples (the deposits of Vishnyakovskoe, East Sayan pegmatite belt and within the Tuyukan ore region, Baikal fold belt) showed open U-Pb system behavior, but selected analyses with the most radiogenic Pb isotopic compositions allowed for reliable U-Pb and Pb-Pb age determinations. The in situ LA-ICPMS ages of 1848 ± 17 Ma (Pb-Pb) to 1835 ± 33 Ma (U-Pb) for cassiterite from the Vishnyakovskoe deposit are within uncertainty of the 1838 ± 3 Ma ID-TIMS age of manganotantalite from this deposit [48]. Published Rb-Sr ages of ~1.5 Ga for pegmatites of the Vishnyakovskoe deposit [49] are ~350 Ma younger than the U-Pb age of 1838 ± 3 Ma of manganotantalite separated from the ore [48] and of the 1.83–1.85 Ga age of cassiterite (this work). The observed disturbance of the Rb-Sr isotope system may be caused by processes that also caused the observed partial disturbance of U-Pb isotope systems in cassiterite.

Similar Paleoproterozoic ages of 1861 ± 12 Ma (Pb-Pb) and 1846 ± 31 Ma (U-Pb) are obtained for combined cassiterite data for four samples from tin deposits in the Tuyukan ore region located in the Baikal-Patom fold-thrust belt. These ore deposits also occur in a region with protracted geologic history and observed disturbance of U-Pb isotope systems in cassiterite from these deposits may be caused by superimposed metamorphic processes [16]. Some degrees of U-Pb systems disturbance were also found in cassiterite samples from the Neoproterozoic Mokhovoe deposit in the Muya district where younger superimposed magmatic processes were dated by U-Pb ID-TIMS method at ~280 Ma [85].

Cassiterite samples from Mesoproterozoic skarn deposits in the Pitkäranta Mining District show no obvious signs of open-system behavior and essentially all the spot analyses were usable for age calculations. Similarly, much younger cassiterite from Cretaceous deposits Valkumei and Merek in the Russian North East and Far East, respectively, shows well-behaved closed U-Pb systematics.

Recalculated published data for cassiterite spot analyses of sample SPG from the Old Mine Field of the Pitkäranta Mining district yield an average age value of 1541.2 ± 9.3 Ma (2 SD) for $^{208}Pb/^{206}Pb$-$^{207}Pb/^{206}Pb$ inverse isochron ages determined in 103 analytical sessions. Similar ages were obtained during this study for two additional cassiterite samples from this ore field (Samples 31 and LA-1, Table 1) and for three cassiterite samples from the ore deposit Kitelä (samples O-4-11, VSH-5, and X-146, Table 1). The age for sample LA-1, separated from a quartz-carbonate metasomatite developed over a Px-Gar skarn (Old Mine Field), is within uncertainty of the other samples from the skarn deposits in this mining district. The large age uncertainties do not allow determining a potential time gap between the skarn formation and the superimposed metasomatic process and indicate that it would not exceed ~20–30 Ma. Sample LA-1 has much lower U concentration compared to other samples from the Pitkäranta skarns, which agrees with previously described lower

U content in recrystallized (younger) cassiterite that was observed in the Sullivan SEDEX deposit in Canada [59].

Two cassiterite samples from tin-bearing metasomatites from the Mokhovoe deposit in the Muya District of Buratia yielded Neoproterozoic ages of 798 ± 19 to 821 ± 27 Ma (Table 1). Much younger ages of 108.3 ± 2.2–108.4 ± 2.2 Ma and 92.6 ± 1.9–93.8 ± 2.1 Ma were obtained for cassiterite from deposits Valkumei (Russian North East) and Merek (Russian Far East), respectively.

The data discussed in this paper show that the inverse $^{208}Pb/^{206}Pb$-$^{207}Pb/^{206}Pb$ isochron approach can be successfully applied to dating older (Proterozoic) cassiterite using spot analyses with low (<0.01) $Th/^{206}Pb$ ratios. Considering the highly variable Th concentrations in cassiterite, a large number of spot analyses was needed to discover the ones with suitable low $Th/^{206}Pb$. The T-W isochron approach also required screening of the data to select analyses with the most radiogenic Pb isotopic compositions. The spot analyses plotting close to the T-W Concordia lower intercept are less sensitive to potential Pb_c heterogeneity and can be used to calculate more accurate anchored T-W isochron ages and ^{207}Pb-corrected $^{206}Pb^*/^{238}U$ ages.

5.3. Relation of Tin Mineralization with Granitic Magmatism

Primary Sn mineralization is commonly spatially associated with felsic magmatic rocks that are interpreted to be the source of these metals (e.g., [86–92]). Common to these magmatic rocks is that they are highly fractionated and show a pronounced enrichment in Sn, W, Be, Cs, F, B, Li, Rb, Ta, and U, and a marked depletion in Fe, Ti, Mg, Ca, Sr, Eu, Ba, and Zr (e.g., [90,91,93–96]). Tin and W mineralization related to felsic magmatic rocks form a variety of deposit types, including greisen, quartz veins, skarn, and less commonly porphyry-type occurrences and pegmatites (e.g., [88,92,97–100]). In addition to Sn and W, the mineralization also may contain economically important amounts of Ta, Nb, Li, B, Ge, Ga, In, and Sc [101–106]. Geochemically related to Sn and W granites are lithium-cesium-tantalum (LCT) type pegmatites, which generally do not show significant Sn and W mineralization, but contain variable, and in part, economically significant amounts of Ta, Nb, Li, Rb, Cs, Be, and Ga (e.g., [107–111]).

The deposits studied in this paper differ in age, type (greisen, skarn, vein, etc.), composition, in the nature of the associated igneous rocks, and in their geodynamic settings. All of the deposits are spatially and genetically related to granitic plutons. The cassiterite age of 1834–1848 Ma from the Vishnyakovskoe deposit is very close to the age of the associated granite of the Sayan complex (1869 ± 6 to 1855 ± 5 Ma [48]). This deposit also contains economically significant amounts of Ta and Nb [46]. Cassiterite from tin deposits of the Tyukan ore region is dated at 1.85–1.86 Ga. The deposits are hosted by the ~1.85 Ga Chuya-Kodar tin-bearing S-type granitic rocks [16,40]. Tin-bearing metasomatites of the Mokhovoe deposit are within 820–830 Ma host rocks of the Bambukoy igneous complex which are geochemically similar to S-type granites [60]. Tin-bearing skarns of the Pitkäranta mining district are closely spatially and genetically related to rapakivi granites of the Salmi batholith [25,58]. Tin ores in the Mesozoic Valkumei and Merek deposits are spatially and genetically associated with granitic rocks of the Pevek pluton and Dusse-Alin intrusive complex, respectively. In all the studied deposits, LA-ICPMS U-Pb ages of cassiterite are within error of the available ages of associated granitic rocks; however, the large LA-ICPMS age uncertainties do not allow determination of a potential time gap between the ore formation and magmatic processes. If this gap existed, it would not exceed ~30 Ma for the Vishnyakovskoe deposit and deposits in the Tuykan ore region, 10–15 Ma for the Pitkäranta Mining District and Mokhovoe deposits, and 2–3 Ma for Cenozoic deposits Valkumei and Merek.

6. Conclusions

LA-ICPMS U-Pb and Pb-Pb ages of cassiterite from six ore deposits from Russia located in the Baltic Shield, Eastern Siberia, Russian North East, and the Russian far east range from ~1.85 Ga to ~93 Ma. Regardless of highly variable U concentrations and common Pb abundances, cassiterite produced reliable geochronological information in all the studied ore deposits. The Tera-Wasserburg isochron approach was applied to samples in the whole age range, while inverse $^{208}Pb/^{206}Pb$-$^{207}Pb/^{206}Pb$ isochrons were used for deposits older than ~0.8 Ga deposits. In several cases, excess scatter of data points was observed on the Tera-Wasserburg diagrams, indicating open system behavior (radiogenic Pb loss), formations of younger cassiterite generations, and variable isotopic composition of the common Pb. The best examples of closed U-Pb systems were found in cassiterite from skarn deposits in the Pitkäranta Mining district. These cassiterites are very low in Th and moderately enriched in U which makes them potentially good candidates as matrix-matched references for in situ U-Pb dating of cassiterite. The inverse Pb-Pb isochron approach that uses ^{208}Pb as a common Pb proxy is applicable to spot analyses with $Th/^{206}Pb < 0.01$ for which an input of radiogenic ^{208}Pb is negligible. In many cases, a large number (>50) of spot analyses were needed to select the data with the lowest $Th/^{206}Pb$ values needed for the inverse Pb-Pb isochrons and to select the most radiogenic measured $^{207}Pb/^{206}Pb$ for Tera-Wasserburg isochrons to minimize potential impacts of heterogeneous Pb_c isotopic composition.

All studied ore deposits are spatially associated with granitic igneous rocks. The cassiterite ages are within error of the ages of the dated granites; however, the errors of the in situ LA-ICPMS U-Pb and Pb-Pb age estimates are too large to determine potential age gaps between the intrusions and the ore-forming metasomatism. In many cases the main source of the elevated uncertainties in the LA-ICPMS age determinations is an external reproducibility of secondary matrix-matched standards, which is not better than ~1.6% for U-Pb ages and ~0.6% for Pb-Pb ages. This is the main limitation of LA-ICPMS U-Pb dating for studies requiring precise geochronological results. However, the low cost and high throughput of the method make it an attractive choice for solving many geological problems that do not require very high precision of age determinations.

Supplementary Materials: The following are available online at https://www.mdpi.com/article/10.3390/min11111166/s1, Table S1: NIST-612-corrected data for matrix-matched cassiterite reference material SPG; Table S2: NIST-612- and SPG-corrected secondary matrix-matched reference cassiterite Jian 1; Table S3: LA-ICPMS results of in situ U-Pb dating of cassiterite from several ore deposits in Russia. The LA-ICPMS data for cassiterite unknowns can be also found in [112].

Author Contributions: L.A.N. and A.M.L. conceived the premise of the paper. L.A.N. and R.J.M. were responsible for the data collection and treatment. Writing was led by L.A.N. with discussion and editing provided by all authors. All authors have read and agreed to the published version of the manuscript.

Funding: This research at IPGG was funded by the Scientific Research Project of IPGG RAS grant No. 0153-299-0001.

Acknowledgments: We would like to thank our colleagues Chris Holm-Denoma and Kate Souders for their help in optimizing LA-ICPMS system. We are indebted to Dave Adams who provided generous help at the U.S. Geological Survey Microbeam Lab in Denver, CO, USA. We gratefully acknowledge W. Powell (Brooklyn College-CUNY) and A.V. Tkachev (Vernadsky Geological Museum, Moscow, Russia) for providing cassiterite samples from the Merek and Vishnyakovskoe deposits. The authors are thankful to G.P. Pleskach for preparing map figures for this paper. Special thanks to Kate Souders (U.S. Geological Survey) and the Journal reviewers who provided constructive and thoughtful reviews of this manuscript. Any use of trade, product, or firm names is for descriptive purposes only and does not imply endorsement by the U.S. Government.

Conflicts of Interest: The authors declare no conflict of interest.

References

1. Yuan, S.; Peng, J.; Hao, S.; Li, H.; Geng, J.; Zhang, D. In situ LA-MC-ICP-MS and ID-TIMS U–Pb geochronology of cassiterite in the giant Furong tin deposit, Hunan Province, South China: New constraints on the timing of tin–polymetallic mineralization. *Ore Geol. Rev.* **2011**, *43*, 235–242. [CrossRef]
2. Zhang, D.; Peng, J.; Coulson, I.M.; Hou, L.; Li, S. Cassiterite U–Pb and muscovite40Ar–39Ar age constraints on the timing of mineralization in the Xuebaoding Sn–W–Be deposit, western China. *Ore Geol. Rev.* **2014**, *62*, 315–322. [CrossRef]
3. Chen, X.-C.; Hu, R.-Z.; Bi, X.-W.; Li, H.-M.; Lan, J.-B.; Zhao, C.-H.; Zhu, J.-J. Cassiterite LA-MC-ICP-MS U/Pb and muscovite 40Ar/39Ar dating of tin deposits in the Tengchong-Lianghe tin district, NW Yunnan, China. *Miner. Depos.* **2014**, *49*, 843–860. [CrossRef]
4. Du, S.; Wen, H.; Qin, C.; Yan, Y.; Yang, G.; Fan, H.; Zhang, W.; Zhang, L.; Wang, N.; Li, H.; et al. Caledonian ore-forming event in the Laojunshan mining district, SE Yunnan Province, China: In situ LA-MC-ICP-MS U-Pb dating on cassiterite. *Geochem. J.* **2015**, *49*, 11–22. [CrossRef]
5. Zhang, R.-Q.; Lu, J.-J.; Wang, R.-C.; Yang, P.; Zhu, J.-C.; Yao, Y.; Gao, J.-F.; Li, C.; Lei, Z.-H.; Zhang, W.-L.; et al. Constraints of in situ zircon and cassiterite U–Pb, molybdenite Re–Os and muscovite 40Ar–39Ar ages on multiple generations of granitic magmatism and related W–Sn mineralization in the Wangxianling area, Nanling Range, South China. *Ore Geol. Rev.* **2015**, *65*, 1021–1042. [CrossRef]
6. Li, C.-Y.; Zhang, R.-Q.; Ding, X.; Ling, M.-X.; Fan, W.-M.; Sun, W.-D. Dating cassiterite using laser ablation ICP-MS. *Ore Geol. Rev.* **2016**, *72*, 313–322. [CrossRef]
7. Cao, H.-W.; Zhang, Y.-H.; Pei, Q.; Zhang, R.-Q.; Tang, L.; Lin, B.; Cai, G.-J. U–Pb dating of zircon and cassiterite from the Early Cretaceous Jiaojiguan iron-tin polymetallic deposit, implications for magmatism and metallogeny of the Tengchong area, western Yunnan, China. *Int. Geol. Rev.* **2016**, *59*, 234–258. [CrossRef]
8. Wang, F.; Bagas, L.; Jiang, S.; Liu, Y. Geological, geochemical, and geochronological characteristics of Weilasituo Sn-polymetal deposit, Inner Mongolia, China. *Ore Geol. Rev.* **2017**, *80*, 1206–1229. [CrossRef]
9. Yan, Q.-H.; Qiu, Z.-W.; Wang, H.; Wang, M.; Wei, X.-P.; Li, P.; Zhang, R.-Q.; Li, C.-Y.; Liu, J.-P. Age of the Dahongliutan rare metal pegmatite deposit, West Kunlun, Xinjiang (NW China): Constraints from LA–ICP–MS U–Pb dating of columbite-(Fe) and cassiterite. *Ore Geol. Rev.* **2018**, *100*, 561–573. [CrossRef]
10. Deng, X.-H.; Chen, Y.-J.; Bagas, L.; Zhou, H.-Y.; Zheng, Z.; Yue, S.-W.; Chen, H.-J.; Li, H.-M.; Tu, J.-R.; Cui, Y.-R. Cassiterite U-Pb geochronology of the Kekekaerde W-Sn deposit in the Baiganhu ore field, East Kunlun Orogen, NW China: Timing and tectonic setting of mineralization. *Ore Geol. Rev.* **2018**, *100*, 534–544. [CrossRef]
11. Zhang, R.; Lu, J.; Lehmann, B.; Li, C.; Li, G.; Zhang, L.; Guo, J.; Sun, W. Combined zircon and cassiterite U–Pb dating of the Piaotang granite-related tungsten–tin deposit, southern Jiangxi tungsten district, China. *Ore Geol. Rev.* **2017**, *82*, 268–284. [CrossRef]
12. Zhang, R.; Sun, W.; Li, C.; Lehmann, B.; Seltmann, R. Constraints on tin mineralization events by cassiterite LA-ICP-MS U–Pb dating. In Proceedings of the 14th SGA Biennial Meeting, Quebec City, QC, Canada, 20–23 August 2017; Volume 3, pp. 1009–1012.
13. Neymark, L.A.; Holm-Denoma, C.S.; Moscati, R.J. In situ LA-ICPMS U–Pb dating of cassiterite without a known-age matrix-matched reference material: Examples from worldwide tin deposits spanning the Proterozoic to the Tertiary. *Chem. Geol.* **2018**, *483*, 410–425. [CrossRef]
14. Moscati, R.J.; Neymark, L.A. U–Pb geochronology of tin deposits associated with the Cornubian Batholith of southwest England: Direct dating of cassiterite by in situ LA-ICPMS. *Miner. Depos.* **2019**, *55*, 1–20. [CrossRef]
15. Lehmann, B.; Zoheir, B.A.; Neymark, L.A.; Zeh, A.; Emam, A.; Radwan, A.M.; Zhang, R.; Moscati, R.J. Monazite and cassiterite U Pb dating of the Abu Dabbab rare-metal granite, Egypt: Late Cryogenian metalliferous granite magmatism in the Arabian-Nubian Shield. *Gondwana Res.* **2020**, *84*, 71–80. [CrossRef]
16. Neymark, L.A.; Holm-Denoma, C.S.; Larin, A.M.; Moscati, R.J.; Plotkina, Y.V. LA-ICPMS U-Pb dating reveals cassiterite inheritance in the Yazov granite, Eastern Siberia: Implications for tin mineralization. *Miner. Depos.* **2021**, *56*, 1177–1194. [CrossRef]
17. Gulson, B.L.; Jones, M.T. Cassiterite: Potential for direct dating of mineral deposits and a precise age for the Bushveld Complex granites. *Geology* **1992**, *20*, 355–358. [CrossRef]
18. Carr, P.A.; Zink, S.; Bennett, V.C.; Norman, M.D.; Amelin, Y.; Blevin, P.L. A new method for U-Pb geochronology of cassiterite by ID-TIMS applied to the Mole Granite polymetallic system, eastern Australia. *Chem. Geol.* **2020**, *539*, 119539. [CrossRef]
19. Tapster, S.; Bright, J.W.G. High-precision ID-TIMS cassiterite U–Pb systematics using a low-contamination hydrothermal decomposition: Implications for LA-ICP-MS and ore deposit geochronology. *Geochronology* **2020**, *2*, 425–441. [CrossRef]
20. Rizvanova, N.G.; Kuznetsov, A.B. A New Approach to ID-TIMS U–Pb Dating of Cassiterite by the Example of the Pitkäranta Tin Deposit. *Dokl. Earth Sci.* **2020**, *491*, 146–149. [CrossRef]
21. Anderson, C.S. Tin: U.S. Geological Survey Mineral Commodity Summaries 2017. pp. 174–175. Available online: https://minerals.usgs.gov/minerals/pubs/commodity/tin/mcs-2017-tin.pdf (accessed on 25 September 2021).
22. Ivanov, O.P.; Yeremenko, L.Y.; Voronov, A.I.; Zorin, Y.M.; Kuzovenko, A.I.; Khar'Kevich, K.A.; Kanoatov, S.I. Mineralogy and Technology of New Economic Types of Tin Ores. *Int. Geol. Rev.* **1993**, *35*, 603–612. [CrossRef]
23. Levine, R.M.; Bond, A.R. Tin Reserves and Production in the Russian Federation. *Int. Geol. Rev.* **1994**, *36*, 301–310. [CrossRef]
24. Bortnikov, N.S.; Lobanov, K.V.; Volkov, A.V.; Galyamov, A.L.; Vikent'Ev, I.V.; Tarasov, N.N.; Distler, V.V.; Lalomov, A.V.; Aristov, V.; Murashov, K.Y.; et al. Strategic metal deposits of the Arctic Zone. *Geol. Ore Depos.* **2015**, *57*, 433–453. [CrossRef]

25. Larin, A.M.; Amelin, Y.V.; Neymark, L.A. Age and genesis of complex skarn ores in the Pitkäranta Ore Province. *Geol. Ore Depos.* **1991**, *33*, 15–33. (In Russian)
26. Ishihara, S.; Govenchuk, V.G.; Govenchuk, G.A.; Korostelev, P.G.; Saydayn, G.R.; Semeniak, B.I.; Ratkin, V.V. Mineralization age of granitoid-related ore deposits in the Southern, Russian Far East. *Resour. Geol.* **1997**, *47*, 255–261.
27. Krymsky, R.S.; Gavrilenko, V.V.; Belyatsky, B.V.; Smolensky, V.V.; Levsky, L.K. The age and genesis of the W-Sn mineralization at the Verkhneurmiiskii ore field, Amur Area: Sm-Nd and Rb-Sr isotopic data. *Petrology* **1997**, *5*, 493–501.
28. Sato, K.; Vrublevsky, A.A.; Rodionov, S.M.; Romanovsky, N.P.; Nedachi, M. Mid-Cretaceous episodic magmatism and tTin mineralization in Khingan-Okhotsk volcano-plutonic belt, Far East Russia. *Resour. Geol.* **2002**, *52*, 1–14. [CrossRef]
29. Tikhomirov, P.; Kalinina, E.; Kobayashi, K.; Nakamura, E. Late Mesozoic silicic magmatism of the North Chukotka area (NE Russia): Age, magma sources, and geodynamic implications. *Lithos* **2008**, *105*, 329–346. [CrossRef]
30. Miller, E.L.; Katkov, S.M.; Strickland, A.; Toro, J.; Akinin, V.V.; Dumitru, T.A. Geochronology and thermochronology of Cretaceous plutons and metamorphic country rocks, Anyui-Chukotka fold belt, North East Arctic Russia. *Stephan Mueller Spéc. Publ. Ser.* **2009**, *4*, 157–175. [CrossRef]
31. Gonevchuk, V.G.; Gonevchuk, G.A.; Korostelev, P.G.; Semenyak, B.I.; Seltmann, R. Tin deposits of the Sikhote–Alin and adjacent areas (Russian Far East) and their magmatic association. *Aust. J. Earth Sci.* **2010**, *57*, 777–802. [CrossRef]
32. Sakhno, V.G.; Polin, V.F.; Akinin, V.V.; Sergeev, S.A.; Alenicheva, A.A.; Tikhomirov, P.L.; Moll-Stalcup, E.J. The diachronous formation of the Enmyvaam and Amguema-Kanchalan volcanic fields in the Okhotsk-Chukotka volcanic belt (NE Russia): Evidence from isotopic data. *Dokl. Earth Sci.* **2010**, *434*, 1172–1178. [CrossRef]
33. Chugaev, A.V.; Budyak, A.E.; Chernyshev, I.V.; Dubinina, E.O.; Gareev, B.; Shatagin, K.N.; Tarasova, Y.I.; Goryachev, N.A.; Skuzovatov, S.Y. Isotopic (Sm–Nd, Pb–Pb, and δ34S) and Geochemical Characteristics of the Metasedimentary Rocks of the Baikal–Patom Belt (Northern Transbaikalia) and Evolution of the Sedimentary Basin in the Neoproterozoic. *Petrology* **2018**, *26*, 213–245. [CrossRef]
34. Prokopiev, A.; Borisenko, A.; Gamyanin, G.; Pavlova, G.; Fridovsky, V.; Kondrat'Eva, L.; Anisimova, G.; Trunilina, V.; Ivanov, A.; Travin, A.; et al. Age constraints and tectonic settings of metallogenic and magmatic events in the Verkhoyansk–Kolyma folded area. *Russ. Geol. Geophys.* **2018**, *59*, 1237–1253. [CrossRef]
35. Alekseev, V.I.; Alekseev, I. Zircon as a Mineral Indicating the Stage of Granitoid Magmatism at Northern Chukotka, Russia. *Geosciences* **2020**, *10*, 194. [CrossRef]
36. Volkov, A.V.; Prokofev, V.Y.; Vinokurova, S.F.; Andreevaa, O.V.; Kiseleva, G.D.; Galyamova, A.L.; Murashova, K.Y.; Sidorova, N.V. Valunistoe epithermal Au–Ag Deposit (East Chukotka, Russia): Geological structure, mineralogical–geochemical peculiarities and mineralization conditions. *Geol. Ore Depos.* **2020**, *62*, 97–121. [CrossRef]
37. Tectonic Map of Russia. Scale 1:15,000,000. 2007. Available online: http://neotec.ginras.ru/neomaps/M150_Russia_2007_Tectonics_Tektonicheskaya-karta-rossii.html (accessed on 25 September 2021).
38. Gorelov, V.A.; Larin, A.M. Chapter 4—Ladoga belt. In *Precambrian Ore Deposits of the East European and Siberian Cratons*; Developments in Economic Geology; Rundkvist, D.V., Gillen, C., Eds.; Elsevier: Amsterdam, The Netherlands, 1997; Volume 30, pp. 87–103. Available online: https://www.sciencedirect.com/bookseries/developments-in-economic-geology/vol/30 (accessed on 25 September 2021).
39. Khiltova, V.A.; Pleskach, G.P. Chapter 13—The Pre-Sayan inlier. In *Precambrian Ore Deposits of the East European and Siberian Cratons*; Developments in Economic Geology; Rundkvist, D.V., Gillen, C., Eds.; Elsevier: Amsterdam, The Netherlands, 1997; Volume 30, pp. 249–270. Available online: https://www.sciencedirect.com/bookseries/developments-in-economic-geology/vol/30 (accessed on 25 September 2021).
40. Larin, A.M.; Salnikova, E.B.; Kotov, A.B.; Makarev, L.B.; Yakovleva, S.Z.; Kovach, V.P. Early Proterozoic syn-and postcollision granites in the northern part of the Baikal fold area. *Strat. Geol. Correl.* **2006**, *14*, 463–474. [CrossRef]
41. Larin, A.M.; Kotov, A.B.; Kovach, V.P.; Sal'Nikova, E.B.; Gladkochub, D.P.; Savatenkov, V.M.; Velikoslavinskii, S.D.; Skovitina, T.M.; Rizvanova, N.G.; Sergeeva, N.A.; et al. Rapakivi Granites of the Kodar Complex (Aldan Shield): Age, Sources, and Tectonic Setting. *Petrology* **2021**, *29*, 277–299. [CrossRef]
42. Larin, A.M.; Ritsk, Y.Y.; Sokolov, Y.M. Chapter 17—Baikal-Patom fold belt. In *Precambrian Ore Deposits of the East European and Siberian Cratons*; Developments in Economic Geology; Rundkvist, D.V., Gillen, C., Eds.; Elsevier: Amsterdam, The Netherlands, 1997; Volume 30, pp. 317–362. Available online: https://www.sciencedirect.com/bookseries/developments-in-economic-geology/vol/30 (accessed on 25 September 2021).
43. Rytsk, E.Y.; Kovach, V.P.; Kovalenko, V.I.; Yarmolyuk, V.V. Structure and evolution of the continental crust in the Baikal Fold Region. *Geotectonics* **2007**, *41*, 440–464. [CrossRef]
44. Khanchuk, A.I. (Ed.) *Geodynamics, Magmatism, and Metallogeny of the Russian East*; Dalnauka: Vladivostok, Russia, 2006; 981p. Available online: http://rodionov.fegi.ru/far_east.pdf (accessed on 25 September 2021). (In Russian)
45. Gladkochub, D.; Pisarevsky, S.; Donskaya, T.; Natapov, L.; Mazukabzov, A.; Stanevich, A.; Sklyarov, A.E. The Siberian Craton and its evolution in terms of the Rodinia hypothesis. *Episodes* **2006**, *29*, 169–174. [CrossRef]
46. Makagon, V.M. Evolution of Nb,Ta-oxide mineralization in rare-metal pegmatites of the East Sayan belt, Siberia, Russia. In Proceedings of the Granitic Pegmatites: The State of the Art—International Symposium, Porto, Portugal, 6–12 May 2007. Available online: https://www.fc.up.pt/peg2007/files/makagon.pdf (accessed on 25 September 2021).

47. Odintsova, I.V.; Syzhykh, A.I. Mineral raw material resources of rare and base metals in Eastern Siberia. In *Geology and Mineral Deposits of Eastern Siberia*; Irkutsk University Publishing: Irkutsk, Russia, 2007; pp. 95–101. (In Russian)
48. Salnikova, E.B.; Larin, A.M.; Yakovleva, S.Z.; Kotov, A.B.; Glebovitskii, V.A.; Tkachev, A.V.; Anisimova, I.V.; Plotkina, Y.V.; Gorokhovskii, B.M. Age of the Vishnyakovskoe deposit of rare-metal pegmatites (East Sayan): U-Pb geochronological study of manganotantalite. *Dokl. Earth Sci.* **2011**, *441*, 1479–1483. [CrossRef]
49. Levitsky, V.I.; Reznitsky, L.Z.; Kotov, A.B.; Sal'nikova, E.B.; Bibikova, E.V.; Kirnozova, T.I.; Kovach, V.P.; Kozakov, I.K.; Barash, I.G.; Abramivich, A.G.; et al. The age and geochemistry of post kinematic granitoids of the south Siberia. In Proceedings of the 2nd All-Russian Conference on Isotopic Geochronology, St. Peterburg, Russia, 25–27 November 2003; pp. 278–281. (In Russian)
50. Makagon, V.M.; Lepin, V.S.; Brandt, S.B. Rubidium-strontium dating of rare-metal pegmatites of the Vishnyakovskoe deposit (East Sayan). *Russ. Geol. Geophys.* **2000**, *41*, 1783–1789.
51. Larin, A.M.; Kotov, A.B.; Salnikova, E.B.; Sklyarov, E.V.; Kovach, V.P.; Plotkina, Y.V.; Anisimova, I.V.; Podolskaya, M.M. The Age, Sources, and Tectonic Setting of Tin-Bearing Granites of the Yazovka Complex of the Baikal–Patom Fold-Thrust Belt. *Dokl. Earth Sci.* **2020**, *490*, 55–59. [CrossRef]
52. Khazov, R.A. *Geological Peculiarities of Tin Mineralization in the North Ladoga Region*; Nedra: Leningrad, Russia, 1973; 87p. Available online: http://elibrary.krc.karelia.ru/528/1/%D0%A2%D1%80%D1%83%D0%B4%D1%8B%20%D0%98%D0%93_15.pdf (accessed on 25 September 2021). (In Russian)
53. Trüstedt, O. Die Erzlagerstätten von Pitkäranta am Ladoga-See. Helsingfors, Frenckellska tryckeriaktiebolaget. *Bull. Commision Géol. Finl.* **1907**, *19*, 333.
54. Iossa, G. News of finding tin and copper in Pitkäranta, Finland. *Gorn. Z.* **1834**, *4*, 157–161. (In Russian)
55. Amelin, Y.; Beljaev, A.; Larin, A.; Neymark, L.; Stepanov, K. Salmi Batholith and Pitkaranta ore Field in Soviet Karelia. In *Rapakivi Granites and Related Rocks Symposium*; Haapala, I., Ramo, O.T., Eds.; GSF: Salonsaari, Finland, 1991; p. 57. Available online: https://tupa.gtk.fi/julkaisu/opas/op_033.pdf (accessed on 25 September 2021).
56. Neymark, L.A.; Amelin, V.Y.; Larin, A.M. Pb-Nd-Sr isotopic and geochemical constraints on the origin of the 1.54–1.56 Ga Salmi rapakivi granite—Anorthosite batholith (Karelia, Russia). *Miner. Pet.* **1994**, *50*, 173–193. [CrossRef]
57. Amelin, Y.V.; Larin, A.M.; Tucker, R.D. Chronology of multiphase emplacement of the Salmi rapakivi granite-anorthosite complex, Baltic Shield: Implications for magmatic evolution. *Contrib. Miner. Pet.* **1997**, *127*, 353–368. [CrossRef]
58. Larin, A.M. *Rapakivi Granites and Associated Rocks*; Nauka: St. Petersburg, Russia, 2011; 402p. (In Russian)
59. Slack, J.F.; Neymark, L.A.; Moscati, R.J.; Lowers, H.A.; Ransom, P.W.; Hauser, R.L.; Adams, D.T. Origin of Tin Mineralization in the Sullivan Pb-Zn-Ag Deposit, British Columbia: Constraints from Textures, Geochemistry, and LA-ICP-MS U-Pb Geochronology of Cassiterite. *Econ. Geol.* **2020**, *115*, 1699–1724. [CrossRef]
60. Larin, A.M.; Rizvanova, N.G.; Salnikova, E.B.; Kotov, A.B.; Kovach, V.P.; Rytsk, E.Y. Age of ores of the tin deposit Mokhovoe and associated rock of the Zhanok-Bambukoj volcano-plutonic association (South-Muya Range, North Transbaikalia). In *Rock, Mineral, and Ore-Formation: Progress and Prospective*; IGEM RAN: Moscow, Russia, 2020; pp. 161–164. Available online: http://www.igem.ru/periodic/news/news_20/progress_90.pdf (accessed on 25 September 2021). (In Russian)
61. Kozlov, S.A.; Novchenko, S.A.; Bogach, G.I.; Tombasov, I.A.; Pinaeva, T.A.; Potemkina, L.V.; Yadrishhenskaya, N.G.; Abdukarimova, S.F.; Kurilenko, A.V.; Raitina, N.I.; et al. *Gosudarstvennaya Geologicheskaya Karta Rossijskoj Federatsii, Scale 1:1000,000*; Aldan-Transbaikalia Series; Sheet N_50-Sretensk; Explonatory Note; VSEGEI Cartographic Factory: St. Petersburg, Russia, 2010; 377p. Available online: https://www.geokniga.org/sites/geokniga/files/mapcomments/n-50-sretensk-gosudarstvennaya-geologicheskaya-karta-rossiyskoy-federacii-tret.pdf (accessed on 25 September 2021). (In Russian)
62. Nokleberg, W.J.; Bundtzen, T.K.; Grybeck, D.; Koch, R.D.; Eremin, R.A.; Rozenblum, I.S.; Sidorov, A.A.; Byalobzhesky, S.G.; Sosunov, G.M.; Shpikerman, V.I.; et al. *Metallogenesis of Mainland Alaska and the Russian Northeast*; U.S. Geological Survey Open-File Report 93-339; U.S. Geological Survey: Reston, VA, USA, 1993; 222p. Available online: https://pubs.usgs.gov/of/1993/0339/report.pdf (accessed on 25 September 2021).
63. Lugov, S.F.; Makeev, B.V.; Potapova, T.M. *Regularities of Formation and Distribution of Tin Deposits in the U.S.S.R. Northeast*; Nedra: Moscow, Russia, 1972; 358p. (In Russian)
64. Nokleberg, W.J. (Ed.) *Metallogenesis and Tectonics of Northeast Asia*; U.S. Geological Survey Professional Paper 1765; U.S. Geological Survey: Reston, VA, USA, 2010; 610p. Available online: https://pubs.er.usgs.gov/publication/pp1765 (accessed on 25 September 2021).
65. Nokleberg, W.J.; Bundtzen, T.K.; Dawson, K.M.; Eremin, R.A.; Goryachev, N.A.; Koch, R.D.; Ratkin, V.V.; Rozenblum, I.S.; Shpikerman, V.I.; Frolov, Y.F.; et al. *Significant Metalliferous and Selected Non-Metalliferous Lode Deposits and Placer Districts for the Russian Far East, Alaska, and the Canadian Cordillera*; U.S. Geological Survey Open-File Report 96-513-A; U.S. Geological Survey: Reston, VA, USA, 1996; 385p. Available online: https://pubs.usgs.gov/of/1996/0513a/report.pdf (accessed on 25 September 2021).
66. Miller, E.L.; Verzhbitsky, V.E. Structural studies near Pevek, Russia: Implications for formation of the East Siberian Shelf and Makarov Basin of the Arctic Ocean. *Stephan Mueller Spec. Publ. Ser.* **2009**, *4*, 223–241. [CrossRef]
67. Rodionov, S.M. Mineral deposit research: Meeting the global challenge. In Proceedings of the Eighth Biennial SGA Meeting, Beijing, China, 18–21 August 2005; pp. 1175–1178. Available online: https://www.springer.com/gp/book/9783540279457 (accessed on 25 September 2021).
68. Khanchuk, A.I. *Ore Deposits of Continental Margins*; Dalnauka: Vladivostok, Russia, 2000; pp. 5–34. (In Russian)

69. Gonevchuk, V.G.; Gonevchuk, G.A. Granitoid magmatism and related mineralization in Sikhote Alin. *Resour. Geol.* **1995**, *18*, 135–141.
70. Farmer, C.B.; Searl, A.; Halls, C. Cathodoluminescence and growth of cassiterite in the composite lodes at South Crofty Mine, Cornwall, England. *Miner. Mag.* **1991**, *55*, 447–458. [CrossRef]
71. Lerouge, C.; Gloaguen, E.; Wille, G.; Bailly, L. Distribution of In and other rare metals in cassiterite and associated minerals in Sn ± W ore deposits of the western Variscan Belt. *Eur. J. Miner.* **2017**, *29*, 739–753. [CrossRef]
72. Paton, C.; Hellstrom, J.; Paul, B.; Woodhead, J.; Hergt, J. Iolite: Freeware for the visualisation and processing of mass spectrometric data. *J. Anal. At. Spectrom.* **2011**, *26*, 2508–2518. [CrossRef]
73. National Institute of Standards, Certificate of Analysis Standard Reference Material 612. 1992. Available online: https://www-s.nist.gov/srmors/certificates/612.pdf (accessed on 25 September 2021).
74. Jackson, S.E. Calibration strategies for elemental analysis by LA-ICP-MS. In *Mineralogical Association of Canada Short Course 40*; Mineralogical Association of Canada: Québec, QC, Canada, 2008; Chapter 11; pp. 169–188.
75. Sylvester, P.J. Matrix effects in laser ablation-ICP-MS. In *Mineralogical Association of Canada Short Course 40*; Mineralogical Association of Canada: Québec, QC, Canada, 2008; Chapter 5; pp. 67–78.
76. Jochum, K.P.; Stoll, B. Reference materials for elemental and isotopic analyses by LA–(MC)–ICP–MS: Successes and outstanding needs. In *Mineralogical Association of Canada Short Course 40*; Mineralogical Association of Canada: Québec, QC, Canada, 2008; Chapter 10; pp. 147–168.
77. Souders, A.K.; Sylvester, P.J. Accuracy and precision of non-matrix-matched calibration for lead isotope ratio measurements of lead-poor minerals by LA-MC-ICPMS. *J. Anal. At. Spectrom.* **2010**, *25*, 975–988. [CrossRef]
78. Pietruszka, A.J.; Neymark, L.A. Evaluation of laser ablation double-focusing SC-ICPMS for "common" lead isotopic measurements in silicate glasses and minerals. *J. Anal. At. Spectrom.* **2017**, *32*, 1135–1154. [CrossRef]
79. Ludwig, K.R. *Isoplot/Ex Rev. 3.75—A Geochronological Toolkit for Microsoft Excel*; Special Publication; Berkeley Geochronology Center: Berkeley, CA, USA, 2012; Volume 5, 75p.
80. Tera, F.; Wasserburg, G. U-Th-Pb systematics in three Apollo 14 basalts and the problem of initial Pb in lunar rocks. *Earth Planet. Sci. Lett.* **1972**, *14*, 281–304. [CrossRef]
81. Stacey, J.S.; Kramers, J.D. Approximation of terrestrial lead isotope evolution by a two-stage model. *Earth Planet. Sci. Lett.* **1975**, *26*, 207–221. [CrossRef]
82. Chew, D.; Petrus, J.; Kamber, B. U–Pb LA–ICPMS dating using accessory mineral standards with variable common Pb. *Chem. Geol.* **2014**, *363*, 185–199. [CrossRef]
83. Roberts, N.M.W.; Rasbury, T.; Parrish, R.R.; Smith, C.J.; Horstwood, M.S.A.; Condon, D.J. A calcite reference material for LA-ICP-MS U-Pb geochronology. *Geochem. Geophys. Geosyst.* **2017**, *18*, 2807–2814. [CrossRef]
84. Akinin, V.V.; Miller, E.L.; Gottlieb, E.; Polzunenkov, G. Geochronology and Geochemistry of Cretaceous Magmatic Rocks of Arctic Chukotka: An Update of GEOCHRON2.02012. Available online: https://ui.adsabs.harvard.edu/abs/2012EGUGA.14.3876A/abstract (accessed on 25 September 2021).
85. Kotov, A.B.; Vladykin, N.V.; Yarmolyuk, V.V.; Salnikova, E.B.; Sotnikova, I.A.; Yakovleva, S.Z. Permian age of the Burpala alkaline pluton, Northern Transbaikalia: Geodynamic implications. *Dokl. Earth Sci.* **2013**, *453*, 1082–1085. [CrossRef]
86. Ferguson, H.G.; Bateman, A.M. Geologic features of tin deposits. *Econ. Geol.* **1912**, *7*, 209–262. [CrossRef]
87. Taylor, R. Some observations upon the tin deposits of Australia. *Bull. Geol. Soc. Malays.* **1979**, *11*, 181–207. [CrossRef]
88. Kwak, T.A. *Developments in Economic Geology: W-Sn Skarn Deposits and Related Metamorphic Skarns and Granitoids*; Elsevier: Amsterdam, The Netherlands, 1987; 451p.
89. Heinrich, C. The chemistry of hydrothermal tin(-tungsten) ore deposition. *Econ. Geol.* **1990**, *85*, 457–481. [CrossRef]
90. Lehmann, B. Metallogeny of tin. *Lect. Notes Earth Sci.* **1990**, *32*, 211.
91. Lehmann, B. Formation of tin ore deposits: A reassessment. *Lithos* **2021**, *402–403*, 105756. [CrossRef]
92. Štemprok, M. A comparison of the Krushne Horu-Erzgebirge (Check Republic-Germany) and Cornish (UK) granites and their related mineralization. *Proc. Ussher Soc.* **1995**, *8*, 347–356.
93. Stussi, J.-M. Granitoid chemistry and associated mineralization in the French Variscan. *Econ. Geol.* **1989**, *84*, 1363–1381. [CrossRef]
94. Breiter, K.; Forster, H.-J.; Seltmann, R. Variscan silicic magmatism and related tin-tungsten mineralization in the Erzgebir-ge-Slavkovsky les metallogenic province. *Miner. Depos.* **1999**, *34*, 505–521. [CrossRef]
95. Bouchot, V.; Ledru, P.; Lerouge, C.; Lescuyer, J.-L.; Milesi, J.-P. 5: Late Variscan mineralizing systems related to orogenic processes: The French Massif Central. *Ore Geol. Rev.* **2005**, *27*, 169–197. [CrossRef]
96. Breiter, K.; Müller, A.; Leichmann, J.; Gabašová, A. Textural and chemical evolution of a fractionated granitic system: The Podlesí stock, Czech Republic. *Lithos* **2005**, *80*, 323–345. [CrossRef]
97. Plimer, I.R. Fundamental parameters for the formation of granite-related tin deposits. *Geol. Rundsch.* **1987**, *76*, 23–40. [CrossRef]
98. Halter, W.E.; Williams-Jones, A.E.; Kontak, D.J. The role of greisenization in cassiterite precipitation at the East Kemptville tin deposit, Nova Scotia. *Econ. Geol.* **1996**, *91*, 368–385. [CrossRef]
99. Sinclair, W.D.; Gonevchuk, G.; Korostelev, P.G.; Semenyak, B.; Rodionov, S.M.; Seltmann, R.; Stemprok, M. *World Tin and Tungsten Deposit Database*; Open File 7688; Geological Survey of Canada: Ottawa, ON, Canada, 2014. [CrossRef]
100. Jingwen, M.; Yanbo, C.; Maohong, C.; Pirajno, F. Major types and time–space distribution of Mesozoic ore deposits in South China and their geodynamic settings. *Miner. Depos.* **2013**, *48*, 267–294. [CrossRef]

101. Schwarz-Schampera, U.; Herzig, P.M. Model of Indium Ore Formation. In *Indium*; Springer: Berlin/Heidelberg, Germany, 2002. [CrossRef]
102. Breiter, K.; Förster, H.-J.; Škoda, R. Extreme P-, Bi-, Nb-, Sc-, U- and F-rich zircon from fractionated perphosphorous granites: The peraluminous Podlesí granite system, Czech Republic. *Lithos* **2006**, *88*, 15–34. [CrossRef]
103. Breiter, K. Nearly contemporaneous evolution of the A- and S-type fractionated granites in the Krušné hory/Erzgebirge Mts., Central Europe. *Lithos* **2012**, *151*, 105–121. [CrossRef]
104. Kempe, U.; Wolf, D. Anomalously high Sc contents in ore minerals from Sn–W deposits: Possible economic significance and genetic implications. *Ore Geol. Rev.* **2006**, *28*, 103–122. [CrossRef]
105. Sinclair, W.; Kooiman, G.; Martin, D.; Kjarsgaard, I. Geology, geochemistry and mineralogy of indium resources at Mount Pleasant, New Brunswick, Canada. *Ore Geol. Rev.* **2006**, *28*, 123–145. [CrossRef]
106. Ishihara, S.; Murakami, H.; Marquez-Zavalia, M.F. Inferred Indium Resources of the Bolivian Tin-Polymetallic Deposits. *Resour. Geol.* **2011**, *61*, 174–191. [CrossRef]
107. Černý, P. Fertile granites of Precambrian rare-element pegmatite fields: Is geochemistry controlled by tectonic setting or source lithologies? *Precambrian Res.* **1991**, *51*, 429–468. [CrossRef]
108. Cerny, P.; Ercit, T.S. The Classification of Granitic Pegmatites Revisited. *Can. Miner.* **2005**, *43*, 2005–2026. [CrossRef]
109. Kontak, D.J. Nature and origin of an lct-suite pegmatite with late-stage sodium enrichment, Brazil lake, Yarmouth county, Nova Scotia. I. Geological setting and petrology. *Can. Miner.* **2006**, *44*, 563–598. [CrossRef]
110. Linnen, R.L.; Van Lichtervelde, M.; Černý, P. Granitic Pegmatites as Sources of Strategic Metals. *Elements* **2012**, *8*, 275–280. [CrossRef]
111. Romer, R.L.; Kroner, U. Phanerozoic tin and tungsten mineralization—Tectonic controls on the distribution of enriched protoliths and heat sources for crustal melting. *Gondwana Res.* **2016**, *31*, 60–95. [CrossRef]
112. Moscati, R.J.; Neymark, L.A. Pb-Pb and U-Pb data of Proterozoic to Phanerozoic Cassiterite Deposits in Russia. U.S. Geological Survey Data Release. 2021. Available online: https://www.sciencebase.gov/catalog/item/612533d8d34e40dd9c03f29c (accessed on 25 September 2021).